AD-A119 575 NAVAL UNDERWATER SYSTEMS CENTER NEW LONDON CT NEW LO--ETC F/G 20/6
PREDICTION OF OPTICAL IMAGE QUALITY NEAR THE SEA SURFACE FROM M--ETC(U)
JUL 82 F S REPLOGLE

UNCLASSIFIED NUSC-TR-6713

NL

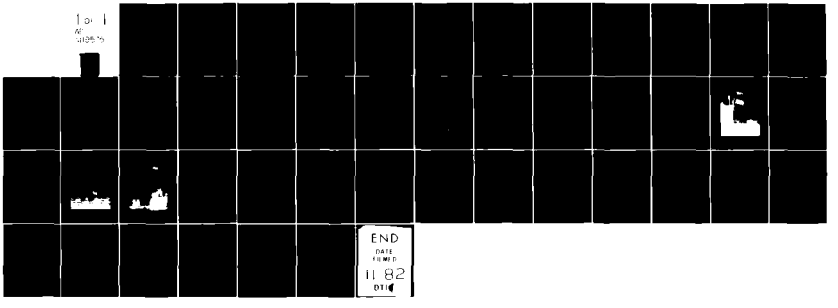

END
DATE FILMED
11 82
DTIC

NUSC Technical Report 6713
13 July 1982

Prediction of Optical Image Quality Near the Sea Surface From Meteorological Measurements

Frank S. Replogle, Jr.
Submarine Electromagnetic
Systems Department

Naval Underwater Systems Center
Newport, Rhode Island / New London, Connecticut

Preface

This work was performed under NUSC Project No. A50040, *Periscope MTF Study — Refractive Irregularity Portion*, Principal Investigator, F. S. Replogle, Jr. (Code 3422), Program Element 61152N, Navy Subproject/Task No. ZR0000101, *Independent Research*, Program Manager, CAPT D. F. Parrish, Naval Material Command (MAT 08L).

This work was a cooperative effort with personnel from the Physics and Meteorology Department of the Naval Postgraduate School of Monterey, California.

The Technical Reviewer of this report was John R. Ball (Code 3422).

Reviewed and Approved: 13 July 1982

W. A. Von Winkle
Associate Technical Director
for Technology

The author of this report is located at the
Naval Underwater Systems Center, New London Laboratory,
New London, Connecticut 06320.

REPORT DOCUMENTATION PAGE		READ INSTRUCTIONS BEFORE COMPLETING FORM
1. REPORT NUMBER TR 6713	2. GOVT ACCESSION NO. AD-A119	3. RECIPIENT'S CATALOG NUMBER 575
4. TITLE (and Subtitle) PREDICTION OF OPTICAL IMAGE QUALITY NEAR THE SEA SURFACE FROM METEOROLOGICAL MEASUREMENTS		5. TYPE OF REPORT & PERIOD COVERED 6. PERFORMING ORG. REPORT NUMBER
7. AUTHOR(s) Frank S. Replogle, Jr.		8. CONTRACT OR GRANT NUMBER(s)
9. PERFORMING ORGANIZATION NAME AND ADDRESS Naval Underwater Systems Center New London, CT 06320		10. PROGRAM ELEMENT, PROJECT, TASK AREA & WORK UNIT NUMBERS 710Y11
11. CONTROLLING OFFICE NAME AND ADDRESS Naval Material Command Washington, DC 20360		12. REPORT DATE 13 July 1982 13. NUMBER OF PAGES 44
14. MONITORING AGENCY NAME & ADDRESS (if different from Controlling Office)		15. SECURITY CLASS. (of this report) Unclassified 15a. DECLASSIFICATION / DOWNGRADING SCHEDULE

16. DISTRIBUTION STATEMENT (of this Report)

Approved for public release; distribution unlimited.

17. DISTRIBUTION STATEMENT (of the abstract entered in Block 20, if different from Report)

18. SUPPLEMENTARY NOTES

19. KEY WORDS (Continue on reverse side if necessary and identify by block number)

Marine Meteorology
Optical Propagation

20. ABSTRACT (Continue on reverse side if necessary and identify by block number)

This report presents a mechanism to calculate the optical index structure constant, C_n^2, from bulk meteorological measurements (air and water temperatures, wind speed, air humidity) made over the ocean. From this, and a formulation of the near-field optical propagation from an incoherent point source, the expected line spread function for near-the sea-surface lines-of-sight are calculated. Finally, three series of photographic line-width observations (made during unstable, neutral, and stable atmospheric buoyancy conditions) are compared with calculated line widths. Mean values of observed results agree with the calculations within about 25 percent for

DD FORM 1 JAN 73 1473

20. (Continued)

conditions of strong atmospheric instability. Since comparisons were made over a variety of target ranges, wind speeds, and camera elevations, it is concluded that the formulations derived are accurate to at least ± 25 percent for conditions of strong atmospheric instability.

Observations made under conditions of neutral and stable atmospheric buoyancy were instrumentally limited to an angular sub-tense of 2 to 4 arc-sec. These measured line-width values fall between 1.9 and 0.6 times the values computed from meteorological measurements.

The variability of image spreading observed across the target fields is indicative of the difficulty of employing a single mechanism to correct for atmospherically induced image-smear.

Table of Contents

List of Illustrations

PREDICTION OF OPTICAL IMAGE QUALITY NEAR THE SEA SURFACE FROM METEOROLOGICAL MEASUREMENTS

INTRODUCTION

The information collection capability of a camera located near the sea surface is limited by the luminance characteristics of the target, the atmospheric path, and the environment. Significant information losses arise from the loss of contrast and picture smearing resulting from the characteristics of the atmosphere along the line-of-sight. Relationships predicting the loss of contrast are relatively well known;[1] however, the relationships between picture smearing (attenuation of optical modulation transfer), sea state, height of the line-of-sight above the surface, and meteorological parameters have only recently been developed. In particular, the formulation of the relationship of the strength of the index structure parameter, C_n^2, to gross meteorological parameters in the near-the-sea-surface environment has been under development only since 1974,[2] and no measurements of C_n^2 have been made closer than 1 m from the sea surface. This independent research effort is one of the first that relates meteorological variables, turbulence, and image smearing for a near-the-sea-surface line-of-sight. The ultimate goal is to be able to predict smearing caused by turbulence, given details concerning the camera, target geometries, and overall meteorology at a particular site.

In a previous NUSC effort,[3] the recording camera was located in a tent on a beach. The target was mounted on a ship stationed 2 to 3.7 km away. The effective turbulence level for the integrated line-of-sight was much larger than that measured only over the water. The result was attributed to turbulence generated by breakers and the shore.

In the current effort, the camera equipment was located on an off-shore tower to provide a full over water line-of-sight; meteorological measuring equipment was located nearby (see figure 1*). The meteorological data were primarily macro (bulk) measurements. A few micro measurements were obtained for use in comparison calculations of C_n^2.

A mechanism[4] for deriving values of C_n^2 from bulk meteorological parameters developed at the Naval Postgraduate School is reproduced here. Expected values of the width of the optical line-spread function for incoherent imaging are obtained using C_n^2 values and near-field optical propagation formulations. These are compared with averages of measured line-spread function widths and critiques of experimental results are presented.

*All figures are presented at the end of the text.

The meteorological portion of the study was guided by personnel from the Meteorology and Physics Department of the Naval Postgraduate School, Monterey, CA. The measurements of variables, data reduction, and optical propagation experiments were carried out by NUSC personnel.

TURBULENCE THEORY

Structure Functions

In turbulence produced by shear flow, the initial power input is into large eddies. This power is then transferred from larger to smaller eddies with little energy loss until it is converted into heat by viscous forces when the eddy sizes approach the inner scale of turbulence l_o (with dimensions of a few millimeters). When the shear is produced by friction in flow parallel to a boundary, the scale size, L_o, of the input eddies at a distance, z, from the boundary is approximately equal to z. For distances r in this inertial range, i.e., $L_o > r > l_o$, we may define a velocity structure function D_v giving the mean square velocity V difference for two points separated by r,

$$D_v(|\vec{r}|) = \langle [V(\vec{0}) - V(\vec{r})]^2 \rangle, \tag{1}$$

where, for simplicity, the definition is expressed in scalar fashion and where, over distances of the order of r, the turbulence is isotropic. (Used properly, D_v is a second rank tensor.) For distances r within the inertial range, the Kolmogoroff or Von Karman spectrum of turbulence element sizes leads to the relationship

$$D_v(r) \sim r^{2/3}. \tag{2a}$$

It has been shown that when gradients of passive additive elements, e.g., temperature, θ, or humidity, Q, exist in the shear flow, the spectra of element sizes lead to similar relationships, i.e.,

$$D_\theta(r) = C_\theta^2 r^{2/3}, \tag{2b}$$

and

$$D_Q(r) = C_Q^2 r^{2/3}, \tag{2c}$$

respectively, where the proportionality constants, C, are *constant* over regions having dimensions of the order of fractions of meters, but may vary slowly over larger distances. Since changes in optical index, n, are related to air density and humidity changes, we have a similar relationship for this variable, i.e.,

$$D_n(r) = C_n^2 r^{2/3}, \tag{3}$$

where C_n^2 has been termed the optical index *structure parameter*.

General Macrometeorological Relationships

The following input variables are used to calculate the strength of C_n^2 from bulk meteorological parameter measurements:

z = height above ocean surface (m),
$T(z)$ = air temperature (°K),
T_0 = water surface temperature (°K),
$q(z)$ = humidity mixing ratio (grams of water/kilogram of air),
q_0 = humidity mixing ratio at sea surface (100% relative humidity at $T = T_0$),
$U(z)$ = wind speed (meters/second), and
P = atmospheric pressure (millibars).

From these one uses the functions

$\theta(z)$ = potential temperature = $T(z) + .01z$,
$\Delta\theta(z)$ = $\theta(z) - T_0$,
$\Delta q(z)$ = $q(z) - q_0$,
ξ = z/L,

where L = Monin-Obukhov scaling length (in meters) is a constant obtained from formulations of $\Delta\theta$, ΔQ, and U.

Since the formulations to be used differ markedly with the convective stability of the atmosphere, we proceed to define stability by

$$\Delta\theta(z) + 6.1 \times 10^{-4} T(z)\, \Delta q(z) > 0 : \text{stable atmosphere},$$
$$\Delta\theta(z) + 6.1 \times 10^{-4} T(z)\, \Delta q(z) < 0 : \text{unstable atmosphere},$$
$$\Delta\theta(z) + 6.1 \times 10^{-4} T(z)\, \Delta q(z) = 0 : \text{neutral atmosphere}.$$

It is then possible[4] to use values of T, T_O, q, U, and P measured at a height of convenience (e.g., 5 to 20 m) in order to obtain a continous formulation giving $C_n^2(z)$. The necessary steps are outlined in the appendix. The resulting expression is

$$C_n^2 = (6.2 \times 10^{-9})\, P^2\, T^{-4} [T_*^2 + 0.070 T_* Q_* + 0.0019\, Q_*^2]\, z^{-2/3} f(z/L), \qquad (4)$$

where

P = pressure (millibars),
T = absolute temperature,
T_*, Q_*, and L are computed in accordance with the appendix,

$$f(z/L) = 4.9\,[1 + 2.4\,(z/L)^{2/3}] \text{ for a stable atmosphere} \qquad (5a)$$

and

$$f(z/L) = 4.9\,[1 - 7\,z/L]^{-2/3} \text{ for an unstable atmosphere}. \qquad (5b)$$

With this formulation of C_n^2, we proceed to determining the effect of turbulence upon imaging over a slant-path above the sea surface.

OPTICAL PROPAGATION AND IMAGING THEORY

Effective Refractive Irregularity Strength Over the Line-of-Sight

To treat the propagation of imaging light from target to camera in the optical *near field,** we assume that the target consists of a series of incoherent point sources of spatially varying intensity. Imaging light from each source then acts independently and travels through the turbulent medium to a camera at a range, R. With a point source, turbulence elements affect the image in accordance with the 5/3 power of the distance from the source.[5,6] Thus, the effective product of the refractive irregularity strength and path length becomes

$$C_n^2(\text{eff})\, R = \int_0^R C_n^2(x)\,(x/R)^{5/3}\,dx, \tag{6}$$

where x is the distance from the source. To simplify the analysis, we assume that the turbulence is uniform over the range, i.e., it is statistically uniform at any particular height, h, above the water, but the average value varies with h, or

$$C_n^2(\text{eff})\, R = \int_0^R C_n^2\,[h(x)]\,(x/R)^{5/3}\,dx. \tag{7}$$

In terms of the geometry illustrated in figure 1,

$$h = h_t - x(h_t - h_c)/R = h_t(1-\alpha x/R), \tag{8}$$

where

h_t = height of target,
h_c = height of camera, and
$\alpha = 1 - h_c/h_t$.

If we use (4) and (5a) for the *stable* atmosphere case, the height dependence of C_n^2 may be expressed by

$$C_n^2(h) = C_n^2(h_m)\,[(h_m/h)^{2/3} + 2.4(h_m/L)^{2/3}] \,/\, [1 + 2.4(h_m/L)^{2/3}], \tag{9}$$

where h_m is the height at which C_n^2 is measured, or derived, from bulk meteorological measurements. Substituting C_n^2 from (9) into (7) and letting $x/R = u$ gives

$$C_n^2(\text{eff})\, R = \left[\frac{R\,C_n^2(h_m)\,h_m^{2/3}}{1+2.4(h_m/L)^{2/3}}\right]\left[\frac{2.4}{L^{2/3}}\cdot\int_0^1 u^{5/3}du + \frac{1}{h_t^{2/3}}\int_0^1 \frac{u^{5/3}\,du}{(1-\alpha u)^{2/3}}\right]$$

$$= \frac{R\,h_m^{2/3}\,C_n^2(h_m)}{1+2.4(h_m/L)^{2/3}}\left[\frac{0.9}{L^{2/3}} + \frac{1}{h_t^{2/3}}\cdot I(\alpha, 0)\right], \tag{10}$$

*In the *near field*, optical propagation wavefront distortions of the receiver are primarily optical phase distortions; in the far field, optical amplitude distortions that cause image scintillation also occur.

where the function

$$I(\alpha,\beta) = (1 + 7\beta)^{2/3} \cdot \int_0^1 \frac{u^{5/3}du}{\{(1-\alpha u)[1 + 7\beta(1-\alpha u)]\}^{2/3}}, \tag{11}$$

with

$$\alpha = 1 - h_c h_t$$
$$\beta = -h_t/L,$$

is shown in figure 2.

For the case of an *unstable* atmosphere, (4) and (5b) give the height dependence of C_n^2 as

$$C_n^2(h) = C_n^2(h_m) \cdot \left[\frac{h_m(1 - 7h_m/L}{h(1 - 7h/L)}\right]^{2/3}. \tag{12}$$

Substituting for h from (8) in (12) and (12) into (7) yields

$$C_n^2(\text{eff})\, R = R\, C_n^2(h_m) \cdot \left[\frac{h_m(1 - 7h_m/L)}{h_t(1 - h_t/L)}\right]^{2/3} \cdot I(\alpha,\beta). \tag{13}$$

Values of $I(\alpha,\beta)$ may be obtained from (11) or from the curves illustrated in figure 2.

Mutual Coherence Function

Yura[7] provides an expression for the averaged mutual coherence function (MCF) of light from an incoherent point source propagated through a *turbulent* atmosphere to an aperture of diameter, D, as

$$M_{st}(\varrho,R) = \exp\{-(\varrho/\varrho_0)^{5/3}[1 - \delta(\varrho/D)^{1/3}]\}, \tag{14a}$$

where

M_{st} = averaged short-term (short-exposure) MCF,

$\varrho = \lambda f F$ = wavelength · camera focal-length · spatial frequency in image plane,

ϱ_0 = long-term (long-exposure) coherence distance

$$= [2.91/2\, C_n^2(\text{eff})\left(\frac{2\pi}{\lambda}\right)^2 R]^{-3/5} \tag{14b}$$
$$= [1.60 \times 10^{14}\, C_n^2(\text{eff}) \cdot R]^{-3/5},$$

$\lambda = 6 \times 10^{-7}$ m (approximately), and

δ = multiplier in the range from 0.5 to 1.0 depending upon the target range.*

*The 0.5 value corresponds to far-field imaging and 1.0 corresponds to near-field imaging. (If $\varrho_0 << \lambda R$, imaging is far field. If $\varrho_0 >> \lambda R$, imaging is near field.) For our case, we used *the multiplier* 0.75 in all the calculations, except the 1980 series. Since the atmosphere was neutral then, imaging was near field and $\delta = 1.0$.

Camera Line-Spread Function

Equation (14a) is also in the form of a statistically-averaged modulation transfer function (MTF) for the cone of atmosphere from the receiving aperture to a target point. To obtain the MTF for the full recording system (MTF_{sys}) we multiplied the atmospheric response by the (approximated) frequency response, H, of an ideal telescope having an 86 mm window and 25 mm obscuration and by an approximation to the frequency response, J, of Pan-X film obtained from a handbook graph. Then substituting 6×10^{-7}m for λ and 1.47 m for f gives, for the overall response,

$$MTF_{sys}(F,\varrho_0) = \exp[-8.8 \times 10^{-7} \cdot (F/\varrho_0)^{5/3} \cdot (1-0.0219\delta \cdot F^{1/3})] \cdot H(F) \cdot J(F), \qquad (15)$$

where $\varrho_0(C_n^2,R)$ was defined in (14b),

$H = F/60{,}000$ if $0 < F \leq 30{,}000$
$H = 1.0/1.4 - F/140{,}000$ if $30{,}000 < F \leq 100{,}000$
$H = 0$ if $F > 100{,}000$, and
$J = [1 + 3(F/53{,}000)^2]^{-1/2}$,

where the units of F are cycles/m.

To compare empirical with theoretical results, one might Fourier transform the observed image-spread functions and compare the averaged transforms with (15). Rather than perform the required multiplied measurements and transforms, we Fourier transformed (15) to obtain expected average line-spread functions for a variety of ϱ_0 values and for $\delta = 0.75$ and 1.0. Figure 3 provides smoothed curves showing the values of line widths (1/e × peak amplitude) that were obtained. They were used to determine expected line widths.

EXPERIMENTAL ARRANGEMENT

The line-of-sight from the target to the camera was as shown in figure 1. The camera, a Questar telescope coupled to a Nikon 35 mm camera back, was attached to a tower corner-post at a various heights, h_c, above the mean water level. The target consisted of a series of five, 1000 W quartz-iodide bulbs, each having a luminous area of 160 by 1.0 mm. The target was placed at a variety of heights, h_t at ranges, R, from 460 to 5000 m.

The meteorological measuring equipment was located on an adjacent corner of the tower in the 1978 observation series and on a mast rigged on the bow of a freighter (the YFRT-287) in the 1980 and 1981 series. The YFRT-287 was anchored 460 m from the tower, just downwind from the camera's line-of-sight. The equipment consisted of an anemometer and wind vane, dew point, air-water temperature difference, and water temperature measuring apparatus. The in-air sensors were located 5.7 m above the water level in the 1978 series and 7 and 8.1 m above in 1980 and 1981. Water temperature measurements were of the *bucket* variety.

In the 1980 observation series, a micrometeorological differential air temperature measuring probe (Contel, Inc., Model MT-2) and a recorder were mounted on the tower. The measurements allowed values for the temperature structure function of the air to be obtained directly. These were convertible to the optical index structure function needed to describe and calculate optical image propagation. This apparatus was used during the data collection effort of 16 May 1980. The results obtained were compared with values of C_n^2 deduced from bulk meteorological measurements made simultaneously. When we attempted to use the micrometeorological measuring apparatus on the primary data collection exercise of 6 June 1980, the fragility of the probes and the lack of a sufficient number of spares limited our data to four single measurements.

Unfortunately, the air-water differential temperature and micrometeorological apparatus failed to operate during the 1981 data collection series. The air-water differential temperature apparatus was replaced with a thermometer located on the shaded side of the ship's mast and another in a bucket in the water.

Accuracy limitations of the sensors were approximately

Static camera resolution (with Pan-X film)	2.5 arc-sec (equivalent to 18 microns on the film)
Image smearing due to target motion	0.04 arc-sec maximum in 1/250 sec exposure
Luminous target geometrical line width	0.45 arc-sec maximum
Wind speed	0.5 m/sec starting speed; ± 0.5 m/sec running accuracy
Dew point temperature	± 1 °C
Air-water differential temperature (air sensor was aspirated and double-shielded in 1978 and 1980 series)	± 0.1 °C (estimated) for 1978 and 1980 series; ± 0.5 °C (estimated) for 1981 series
Water temperature measuring apparatus	± 1 °C
Differential air temperature measuring apparatus	± 10^{-17} C_n^2 units

DATA COLLECTION AND PROCESSING

General

The three series of observations were made at Brenton Reef Tower, located just off the entrance to Narragansett Bay (see figure 4). We attempted to position the target-carrying ship in a direction such that the camera line-of-sight was normal to the wind direction. Camera and target heights and ranges are given in table 1. In

nearly all cases camera exposure time was 1/1000 sec. To ascertain that critically focused images were obtained, we first determined the relationship between the camera viewer *best focus* and the film *best focus* in the laboratory. Then, in the field, recordings were made at every target range for a series of focus positions bracketing the laboratory-determined best focus position.

Table 1. Geometry for Film Recording

Observation Series	Day	Time	Target Ranges (m)	Mean Height (m)	Camera Height (m)
A	9/26/78	1000-1130	460-2740	6.2	2.4
B	9/26/78	1145-1250	460-2740-460	6.2	1.4
C	9/26/78	1400-1430	460-1830	6.2	1.0
F	9/27/78	1230-1250	2740-460-1830	6.2	2.3
G	9/27/78	1325-1400	460-2740-460	6.2	0.8
H	6/6/80	1055-1305	990-4970-520	9.85	0.9
I	6/6/80	1405-1540	950-5145-500	9.85	1.7
J	6/6/80	1600-1715	425-5030-1000	9.85	3.1
K	5/8/81	1005-1118	500-4000-3000	7.9	1.1
L	5/8/81	1130-1215	5000-500	7.9	0.95
M	5/8/81	1235-1402	500-5000-500	7.9	2.0
N	5/8/81	1430-1500	500-5000	7.9	3.3

Bulk meteorological data were taken and recorded continuously during the three expeditions. Recorded results were first averaged for 15 or 30 min periods and the averages were interpolated to provide data for camera image recording times.

The ends of each exposed film strip were given a step-wedge exposure in the laboratory and the film was processed continuously in a Versamat processor. Then, using a microscope and scale, the image negatives were scanned to determine approximate image widths and the best-focus frames. These were then scanned by a Joyce-Loebl Model 3C microdensitometer.* We attempted to choose nominally average portions of the five source images for scanning on the selected frames. This same principle was applied when the images were smeared together because of atmospheric irregularities. The peak density values for all scans were obtained from a (visually) smoothed trace and an averaged background density value was obtained. The density versus exposure transfer (H and D) curve for Pan-X film was obtained from the step wedge exposures and the equivalent peak and background exposures, E_p and E_b, were found. Then, the $1/e^{th}$ signal exposure level, E_{es}, was calculated from

$$E_{es} = (E_p - E_b)/e, \tag{16a}$$

*The formulation $[(\text{measured width})^2 - (\text{scanning slit width})^2]^{1/2}$ was used as a correction factor for the image broadening caused by finite slit width.

and the corresponding exposure with background added was

$$E_c = E_p/e + E_b(1 - 1/e) . \quad (16b)$$

Using the transfer curve again, the image density corresponding to E_e was determined. Then the image width between $1/e^n$ points was measured. Finally, for a particular exposure series and target range, the 1/e image widths were averaged to obtain mean values and expected standard deviations of the mean and individual images were computed.

1978 Observation Series

The first observations were made during very unstable marine atmosphere conditions on 26 and 27 September 1978. Thirty minute averages of recorded meteorological data are illustrated in the eight lower curves of figures 5a and 5b. The sky was completely clear on 26 September. The uppermost curves show the C_n^2 values computed by Naval Postgraduate School personnel for the meteorological apparatus height of 5.7 m.

A total of 411 exposures were made and line widths were measured on 73. Figures 6 and 7 are enlarged prints of *typical* exposures from the first series of observations. In printing, the light source portions of the negatives were masked during most of the exposure to show the structure in the spread functions. Since the exposure times for the negatives were chosen to avoid saturation of the target source portion of the frame, the ship and background are underexposed. The length of the target array is 0.8 m.

1980 Observation Series

The shutter of the Nikon data camera failed to operate during the 16 May 1980 expedition and there were no film exposures. Only the micrometeorological and bulk meteorological measurements obtained were useful. Figure 8 compares values of C_n^2 computed from bulk meteorological measurements with values obtained by the microthermal bridge apparatus.

On 6 June 1980 approximately 460 exposures (images of the target) were made and 98 were scanned by the microdensitometer. Each exposure was scanned about three times to obtain a mean value for the line-image spread on the frame. Thirty-seven were then selected as representative of best focus conditions and, from these, line widths representing the geometrical conditions during data collection were obtained. Figures 9 and 10 are photographs of targets at 1 km and 4.97 km. The quality of the target image in figure 10 should be compared with that in figure 7, which was obtained in the presence of strong turbulence at only 1.83 km.

Values of the measured meteorological variables and computed values of C_n^2 for data taken on 6 June are shown in figure 11. The gaps in the curves represent the time interval when YFRT-287 was transiting to a new anchorage, a move necessitated by an earlier shift in wind direction.

1981 Observation Series

Approximately 400 exposures were made during the 8 May expedition and 77 were scanned by the microdensitometer. Each exposure was scanned about three times and 32 were selected as best focused. Line widths representative of the geometrical conditions of the data were obtained from these.

Values of measured meteorological variables and computed values of C_n^2 are shown in figure 12. During the interval of 0930 to 1115, values of C_n^2 could not be computed from (5a) and (5b) since $\varepsilon_0' > 1.25$, and no formulation for computing C_n^2 from bulk measurements exists for the highly (buoyantly) stable atmosphere indicated.

OBSERVATION RESULTS

The data series are in three categories of atmospheric stability, i.e., unstable, neutral, and stable for 1978, 1980, and 1981, respectively. Thus, the results are presented separately (see figures 13 through 24). The arrows indicate the time sequences in which data were recorded. The line widths represent distances between points on the film having exposure values of $1/e \times$ peak amplitude. Ordinate scales are linear, except for the 1978 data plots which are duplicated with logarithmic ordinates to illustrate the percentage of inaccuracy between computed and measured line width values. The abscissa of each is plotted on a $(\text{range})^{0.6}$ scale since, for a uniformly turbulent path, the image spreading caused by turbulence only is proportional to this function of range (see (24)). Brackets indicate $\pm\ 1\sigma$ values in the measured widths. The solid line brackets show standard deviation values for the means of all the data. Broken line brackets (1978 only) show standard deviations for a single datum. Adjacent numbers provide the number of frames of data used to find the mean and standard deviations. Circles show the mean spread function widths to be expected from computations of C_n^2 and the resulting optical propagation (see (24)). The zero range value was obtained by Fourier transforming the combined camera and film responses given in (21) and (22). The ratios of observed to meteorologically predicted line widths for each range (excluding 500 m range data*) have been averaged geometrically for each figure. This average is represented in the figures by β. Table 2 summarizes factors peculiar to the data groups.

DISCUSSION OF RESULTS

Unstable Atmosphere and Strong Turbulence

Under unstable atmosphere, strong turbulence conditions, the mean values of measured line widths differ, at most, by a factor of two from those predicted from bulk meteorological measurements. This is in approximate agreement with the factor of two accuracy Davidson[4] obtained for the index structure constant from

*We do this because data from the 1978, 1980, and 1981 observation series show excessive line widths for this near range. It must be concluded that factors other than atmosphere lead to this broadening of lines.

Table 2. Factors Specific to Data Groups

Date	Time Interval	Figure No.	Turbulence	Atmospheric Stability	Geometric Mean of β Values	Notes
9/26/78	1000 to 1500	16a to 18b	Very Strong	Unstable	0.84	
9/27/78	1230 to 1400	19a to 20b	Strong	Unstable	1.11	
6/6/80	1055 to 1715	21 to 23	Very Weak	Variable	1.63	The atmosphere was essentially neutral during this time interval.
5/8/81	1005 to 1500	24 to 27	Light	Stable	0.74	Computed line width values are omitted from figure 24 since meteorological parameter readings fell outside the range of possible computation. All computed line width values on figure 27 were obtained from meteorological observations made at 1430.

bulk meteorological measurements.* It is significant that the geometric mean of the ratio of observed to predicted line widths for the full set of data is much closer than this (0.91/1), which indicates that, when space and time variations are averaged, the correspondence of theory with mean turbulence conditions is much closer. Close attention to ambient conditions (figure 6 presents 30 min averages) shows that the wind speed was highly variable between 1200 and 1500 on September 26. The β values for data series B and C (figures 15 and 16) between 1145 and 1250 and 1400 and 1430 are 0.85 and 0.60, giving a geometric mean of 0.71; whereas the values for data series, A, F, and G, are 1.17, 1.01, and 1.04 giving a geometric mean of 1.07.

We noted that for single-line width observations, an aspect that has not been treated theoretically, the 1σ fractional deviation from the mean, averaged over the set of ranges (excluding 460 m) and times, was 34 percent of the mean. The maximum 1σ value at maximum range was 86 percent.

Neutral Atmosphere

In this series of observations, the measured line widths are higher than those calculated and, essentially, independent of target range. This points to an instrumental limitation in achievable line width of about 25 to 30 microns.

*A factor of two agreement in line width can be shown to be equivalent to a factor of three agreement in the values of C_n^2.

A correlation of measured line width with computed line width is shown in figure 18 for 2.99 and 4.55 km. The products of C_n^2 (computed for a height of 6.67 m) and ranges were 8.0 and 2.1 $\times$ 10^{-14} $m^{1/3}$, respectively. From these data one concludes that if an ideal camera located 1 m above the sea surface records a ship or shore in a millisecond exposure, the images will have a mean line spread of 2.5 arc sec,* or less, if the two primary ambient conditions are met, i.e., if air temperature - water temperature $\leq$ 1.25 °C (stable atmosphere) and wind speed $\geq$ 2.0 m/sec = 3.9 knots.

We noted that in figures 16b and 17b, where the temperature and wind conditions were stabilized, the $(\text{range})^{0.6}$ dependence of the line width was followed with a deviation of less than 6 percent from 920 to 2740 m. We also compared two measured line width values at 2740 m to check the camera elevation factor. Lowering the camera from a height of 2.3 m to 0.8 m (with C_n^2 values nearly the same) increased the line width by 47 percent. Theoretically this change (allowing for different L values) should be only 40 percent. It was concluded that the camera height formulation was correct because the difference ratio, 1.47/1.40 = 1.05, was so close to 1.

The correspondence between measured mean and theoretical values of line spread suggest that the theoretical formulations are accurate within tens-of-percent for these turbulent conditions at target ranges from 910 to 2740 m, wind speeds from 2 to 7 m/sec, and camera elevations (from the surface of the ocean) between 0.8 to 2.4 m.

Stable Atmosphere and Weak Turbulence

Since the particularly high air-water temperature differences shown in figure 12 (between 0945 and 1100) do not result in the large line widths shown in figure 21 (between 1005 and 1118), it is probable that the back-up therometer was subject to local heating and, thus, was not measuring the true temperature of the air above the ocean. A comparison of wind speed versus time in figure 12 shows that air speed in this time interval was less than 1 m/sec, with the exception of a brief burst at 1030.

The line widths recorded in figure 22 (between 1130 and 1215) appear be the minimum possible given the instrumentation employed except, perhaps, for the 30.6 micron line width at a target range of 5 km at 1130. Generally, the line width values computed theoretically appear to be unduly high. Again, this may be the result of the low wind speed of 1.3 m/sec.

In figure 23 (between 1235 and 1400) the wind had stabilized at 2.5 to 3.5 m/sec, but the measured air-water difference values were from 1/2 to 1 °C too high to permit agreement of measured and computed line width values.

*This value is obtained by rss subtraction of the limiting value of the line width produced by the equipment from the mean measured line width values. It also corresponds approximately with the line width predicted for an ideal camera with a C_n^2 x range product of 8.0 x 10^{-14} $m^{1/3}$ in a stable atmosphere.

The measured and computed line width values shown on figure 24 (excluding the 500 m data) show reasonable agreement. Although the theoretical values are based on only one meteorological measurement set, the 1430 recording, the wind and temperature were stabilized by this time. Thus, the extrapolation of meteorological data to 1500 seems justified. Then assuming that the results shown in figures 23 and 24 are based on reasonably correct data and uniform ambient conditions, one notes that the combined ratio of measured/computed line widths is $(0.61 \times 1)^{1/2} = 0.78$.

GENERAL CONCLUSIONS

For strong turbulence with unstable atmospheric equilibrium, mean line width measurements will match the values computed from bulk meteorological measurements by the formulations provided here to within a few percent. Single line width measurements can differ from the computed values by a factor of two.

When neutral or weakly stable atmospheric conditions ($C_n^2 < 10^{-14}$ m$^{-2/3}$) existed, minimum line width values varying from 3.5 to 4 arc-sec were recorded (a 2.5 arc-sec line width was expected). This seriously limited the accuracy with which results could be related to computed line width values and, thus, the accuracy with which the effects of the turbulence could be inferred. Two sets of mean line widths obtained under atmospherically stable conditions gave combined ratios of measured-to-computed line widths of 0.78/1.0, but turbulence contributions to the line widths were too small to develop conclusions concerning the accuracy of the theoretical turbulence formulations.

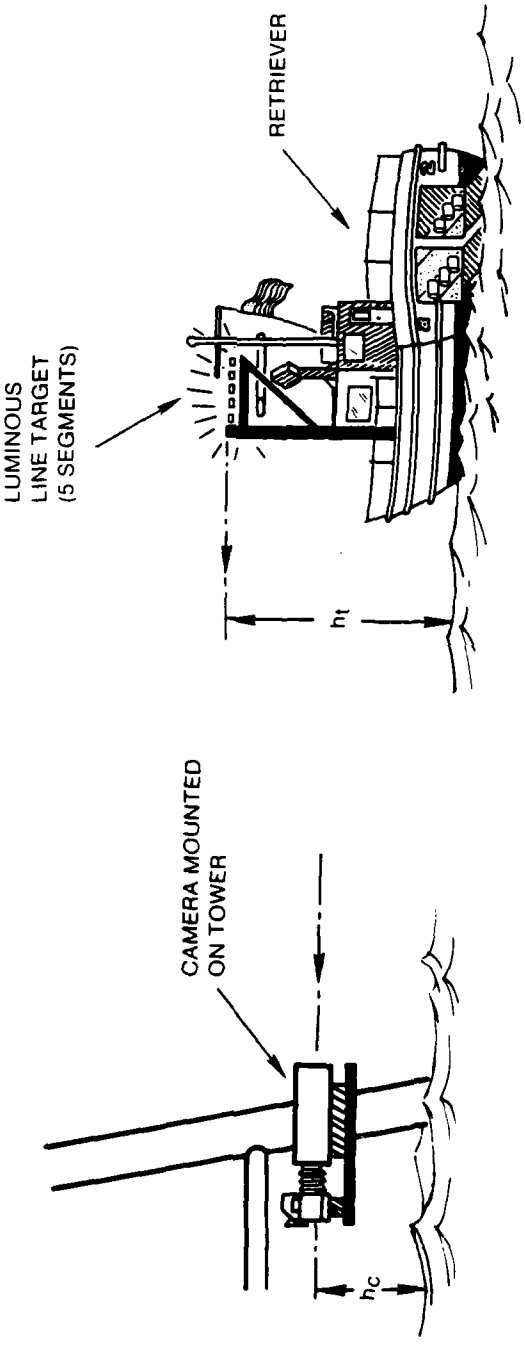

Figure 1. Geometry Used During Collection of Optical Data

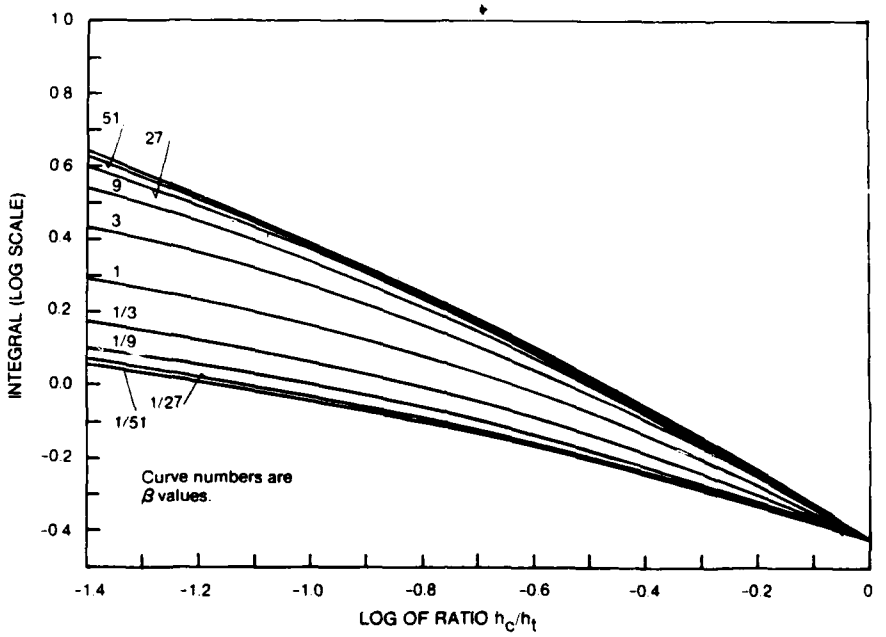

Figure 2. C_n^2(eff) Integral: $I(\alpha,\beta)$

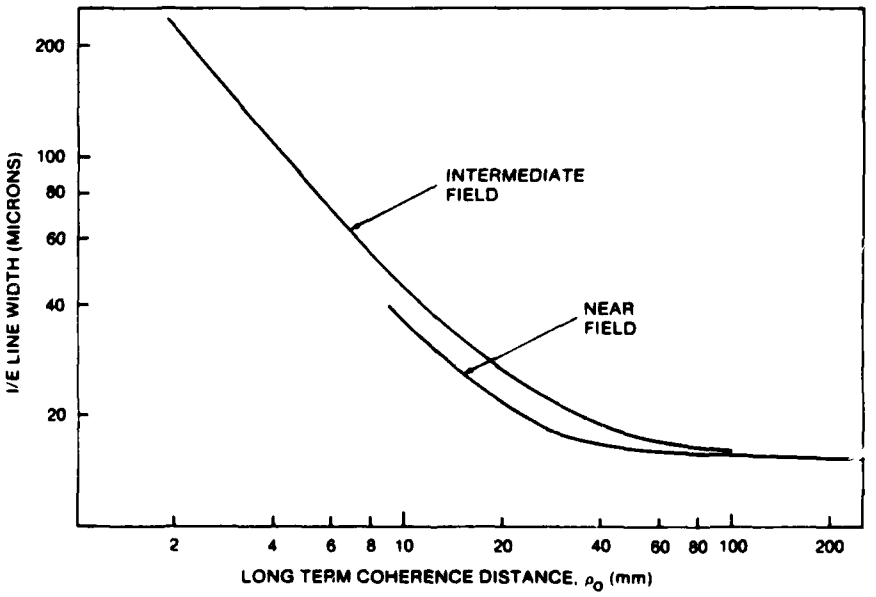

Figure 3. Theoretical Mean Line Widths for Near and Indermediate Field Propagation

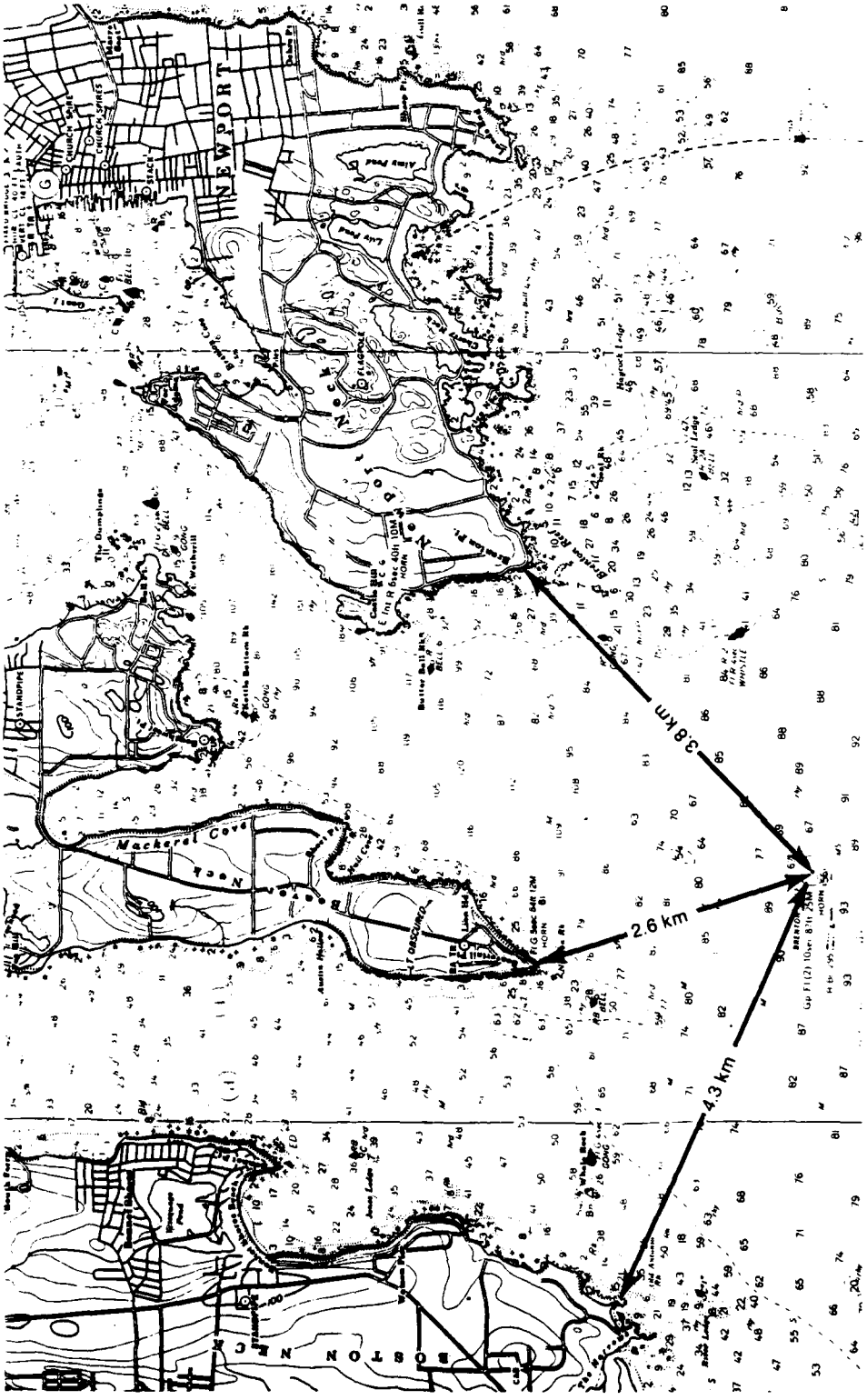

Figure 4. Locaiion of Brenton Reef Tower at the Entrance to Narragansett Bay (Water Depth in Feet)

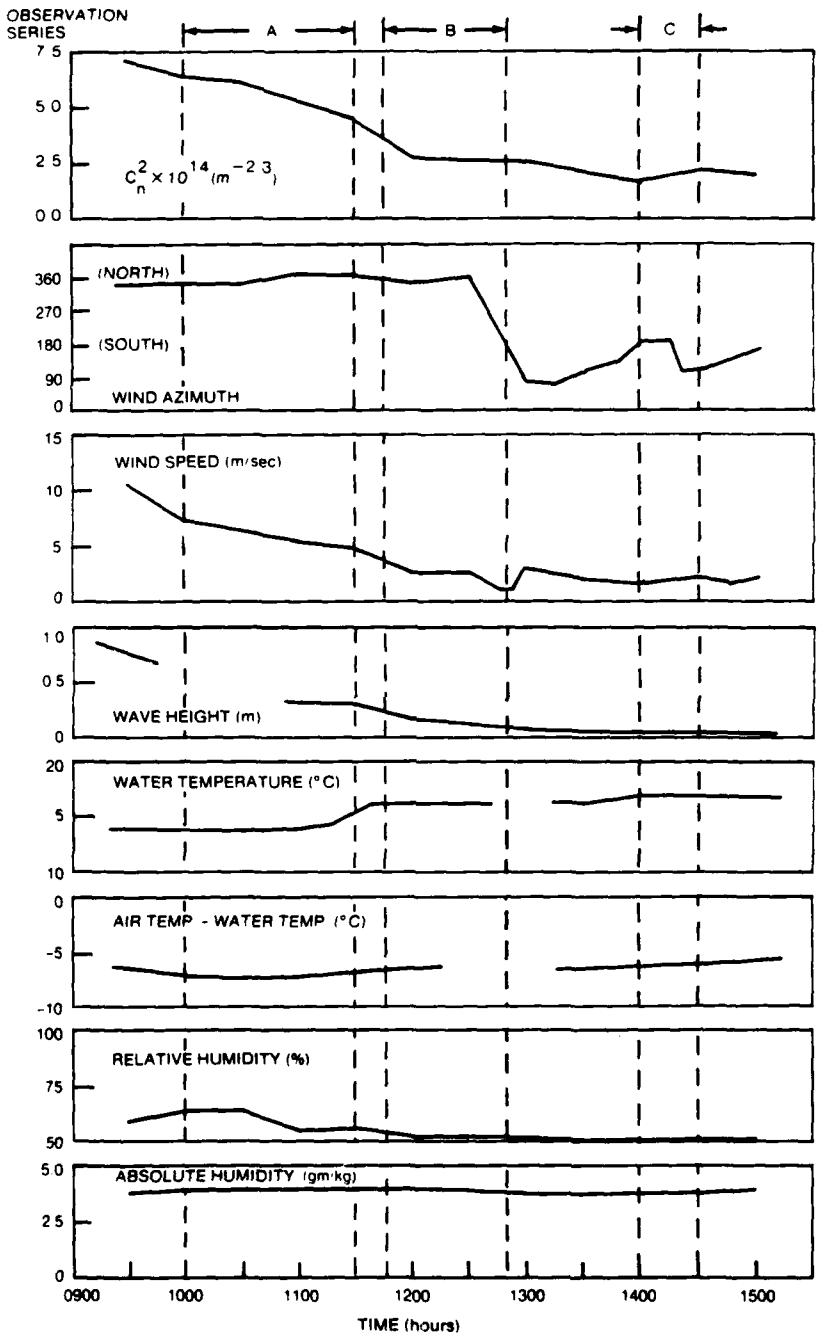

Figure 5a. 26 September 1978 Data and Computed C_n^2

Figure 5. 1978 Meterological Data

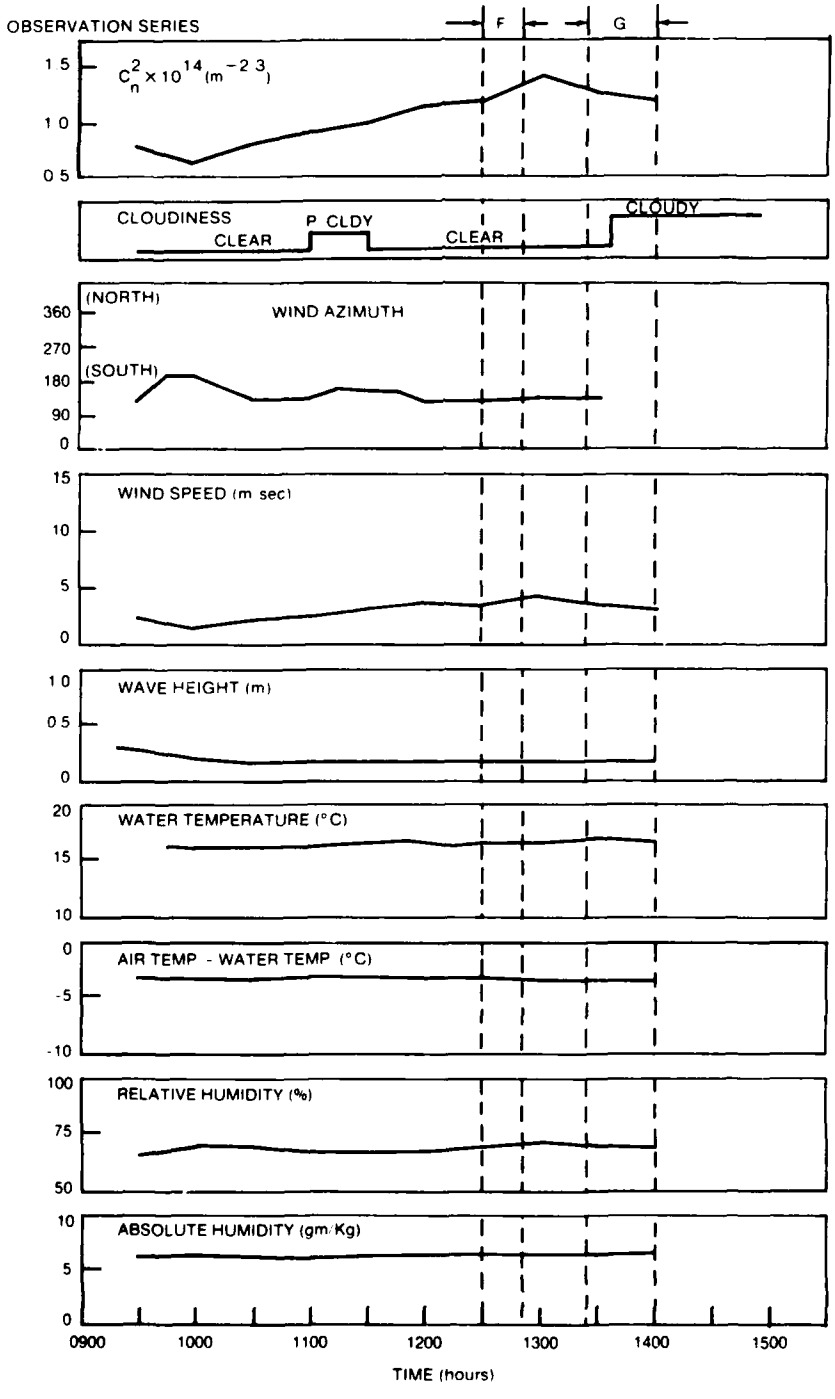

Figure 5b. 27 September 1978 Data and Computed C_n^2

Figure 5. (Cont'd) 1978 Meteorological Data

Figure 6. Enlarged Print of Image Obtained in a Strongly Turbulent Atmosphere at 460 m (C_n^2: 6.4×10^{-14})

Figure 7. Enlarged Print of Image Obtained in a Strongly Turbulent Atmosphere at 1.83 km (C_n^2: 4.4×10^{-14})

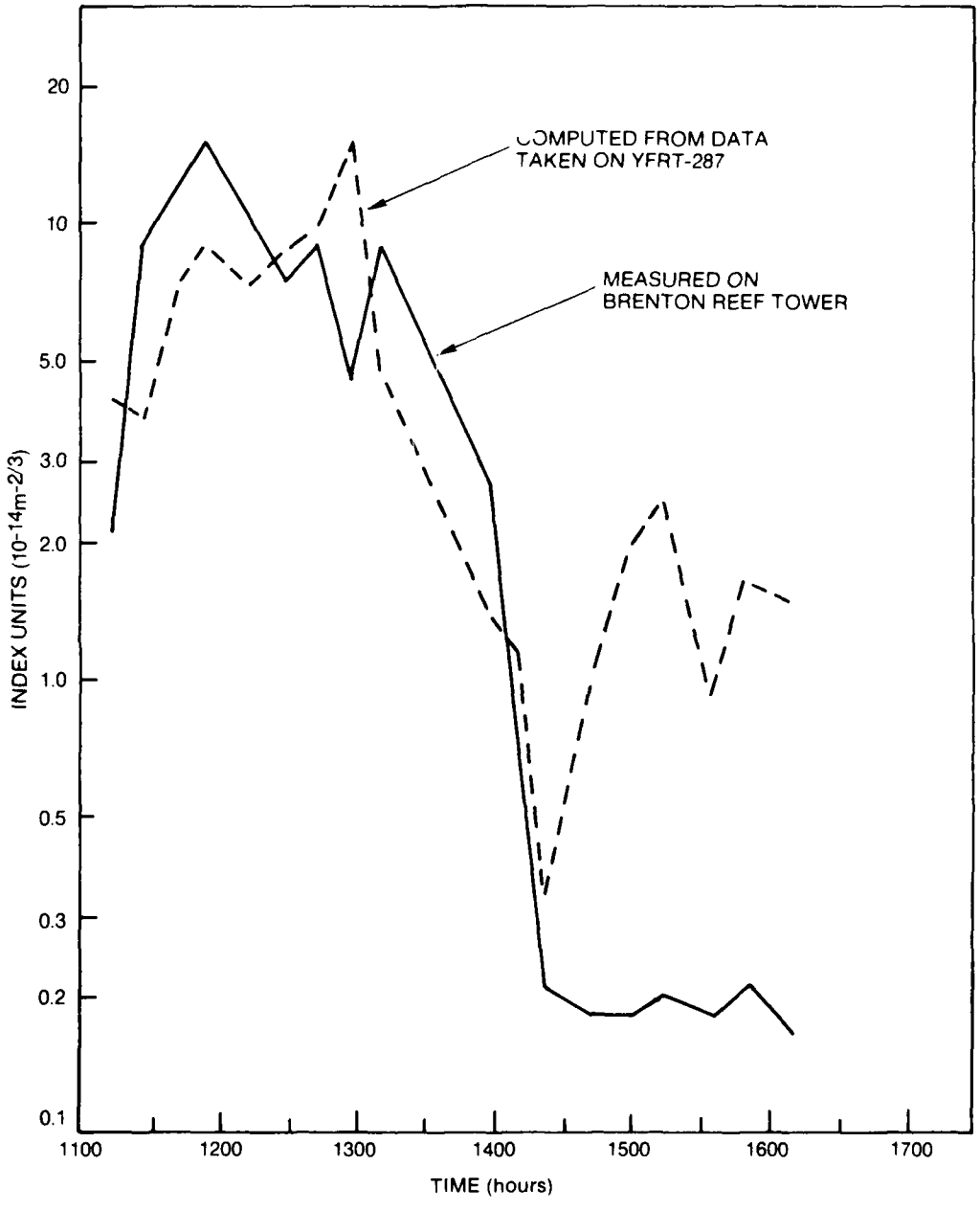

Figure 8. Computed and Measured Values of C_n^2

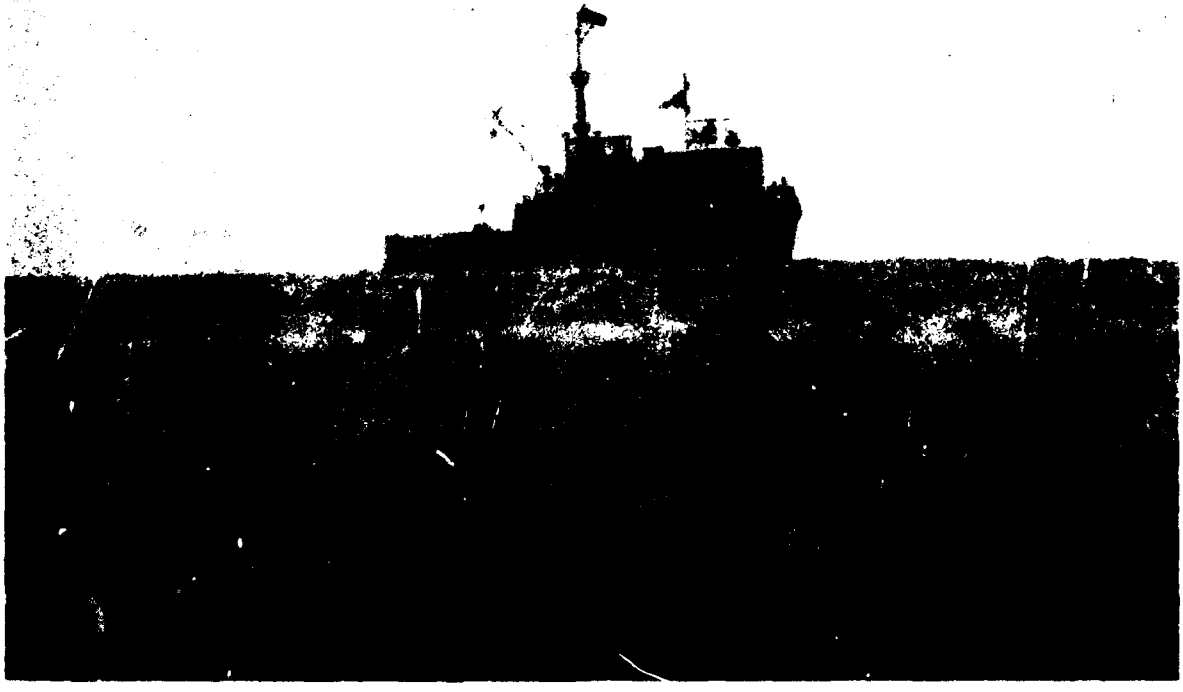

Figure 10. Enlarged Print of Image Obtained in a Weakly Turbulent Atmosphere at 4.97 km (C_n^2: 0.72×10^{-15})

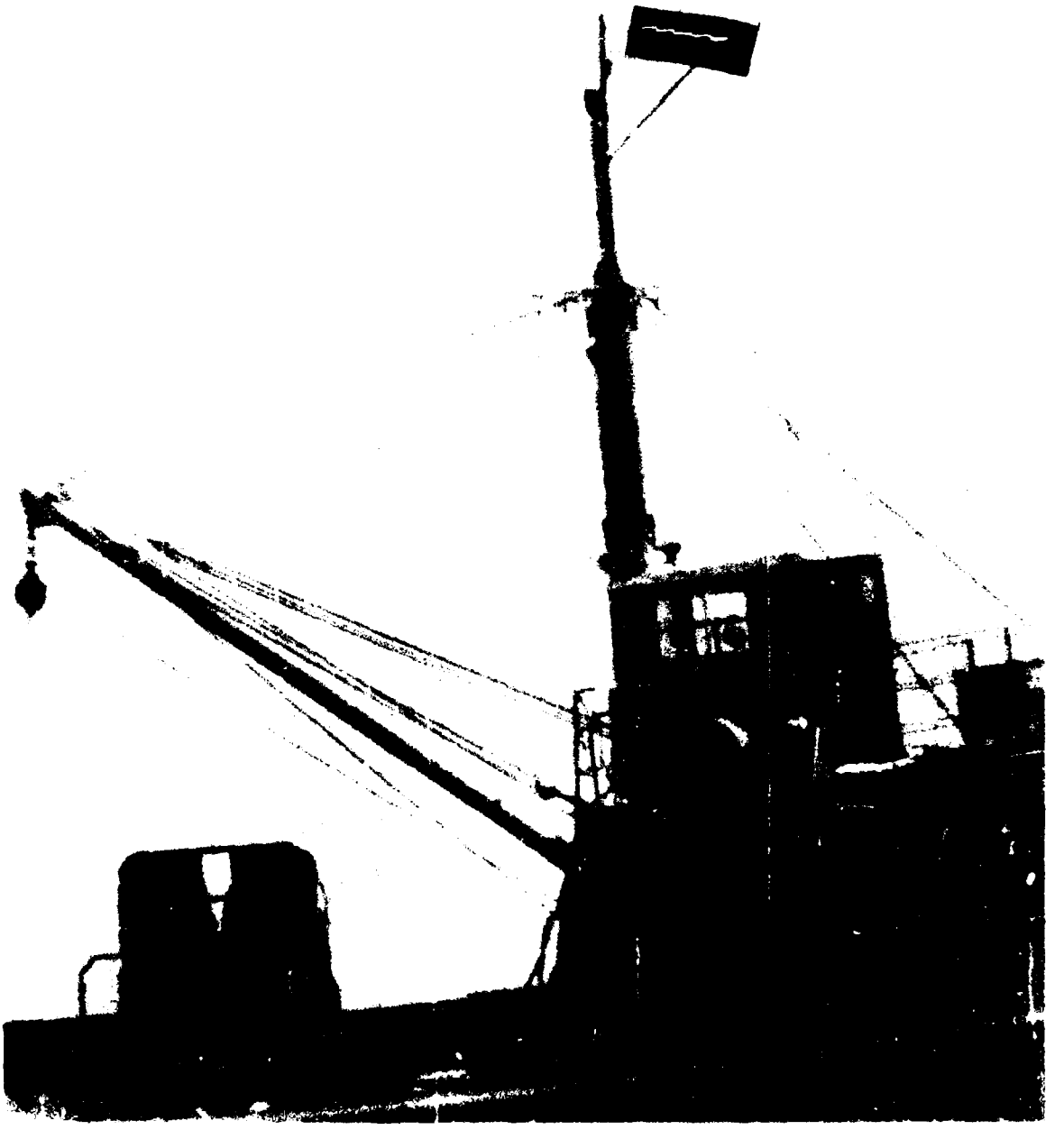

Figure 9. Enlarged Print of Image Obtained in a Weakly Turbulent Atmosphere at 1 km (C_n^2: 2.5×10^{-15})

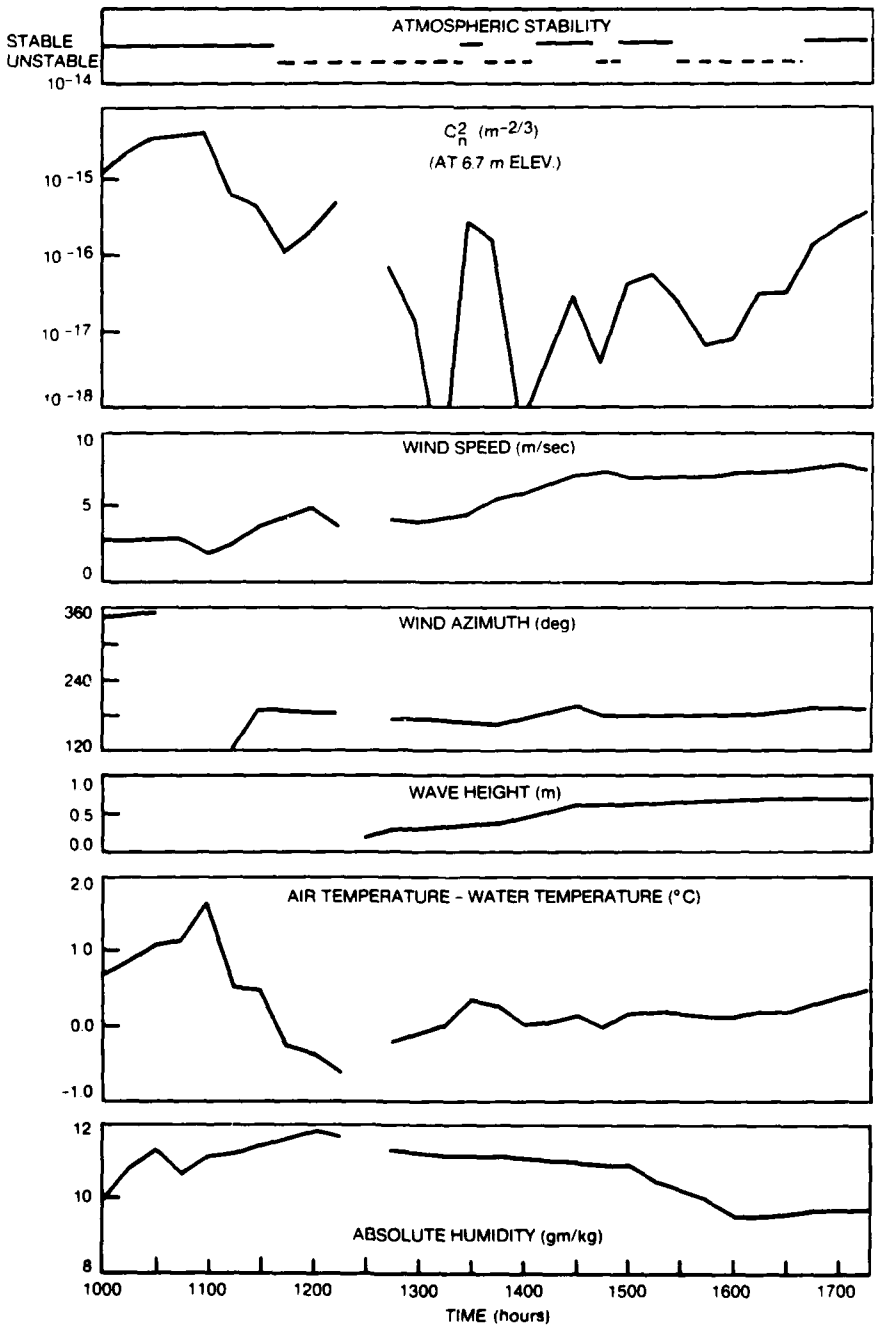

Figure 11. Measured Meteorological Data (6 June 1980) and Computed C_n^2

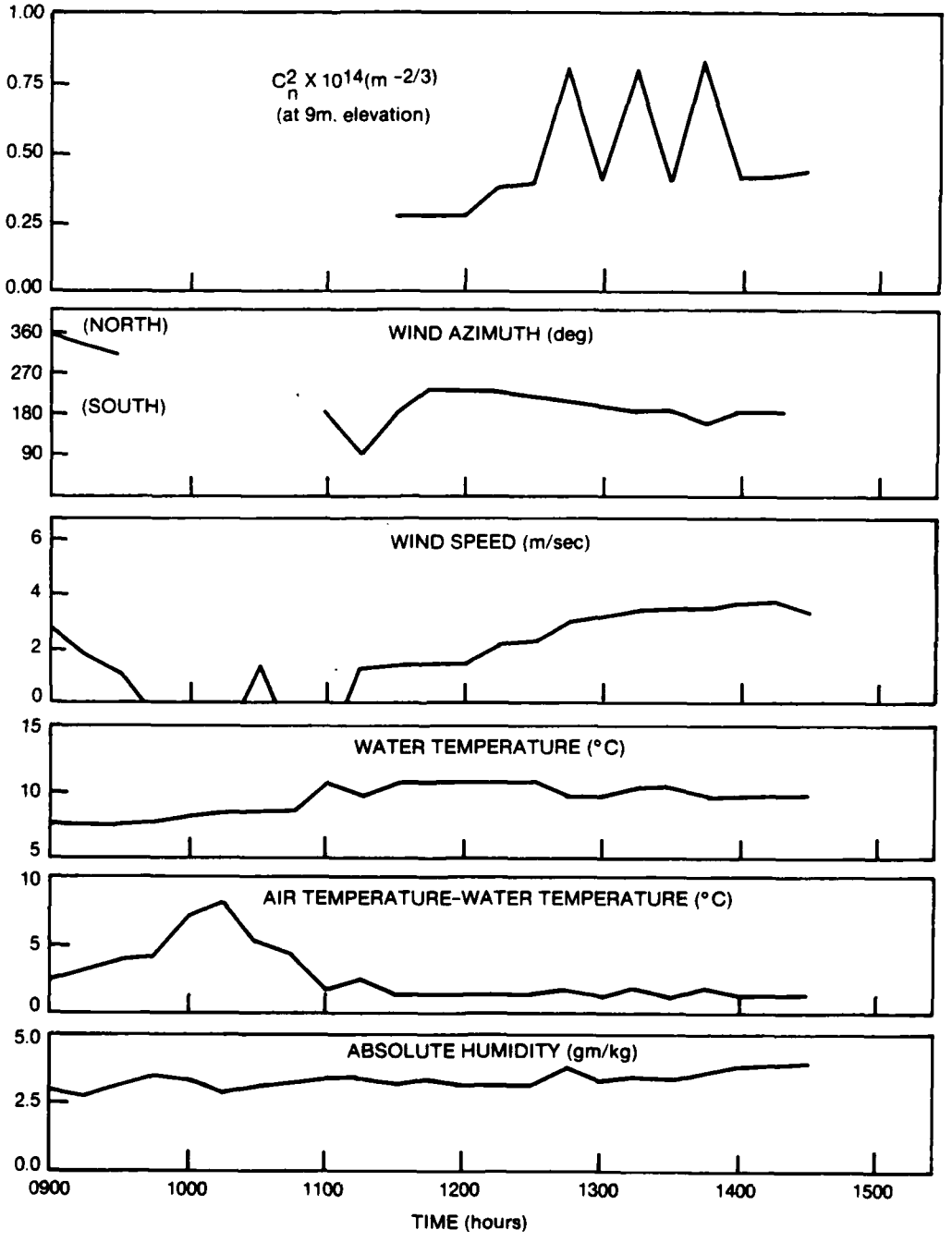

Figure 12. Measured Meteorological Data (8 May 1981) and Computed C_n^2

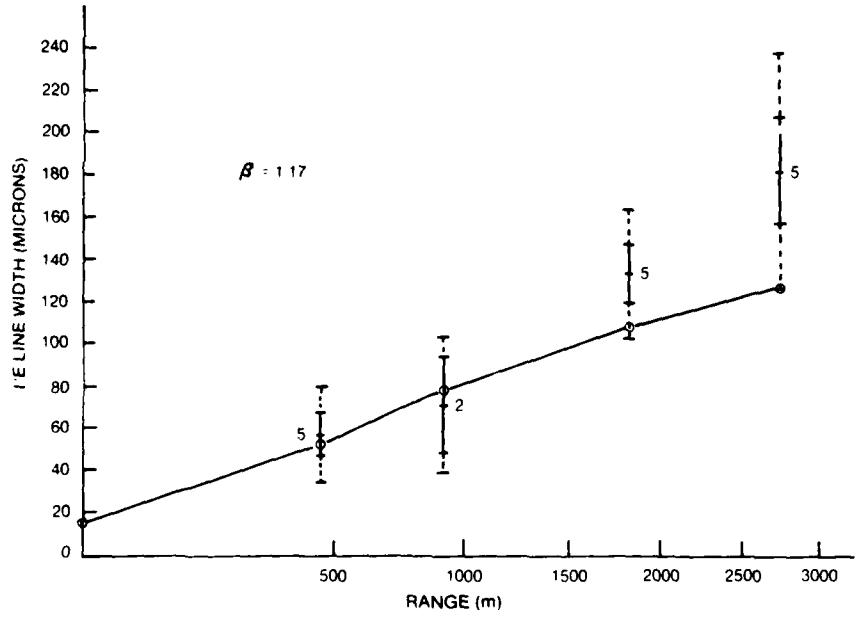

Figure 13a. Line Width (Microns)

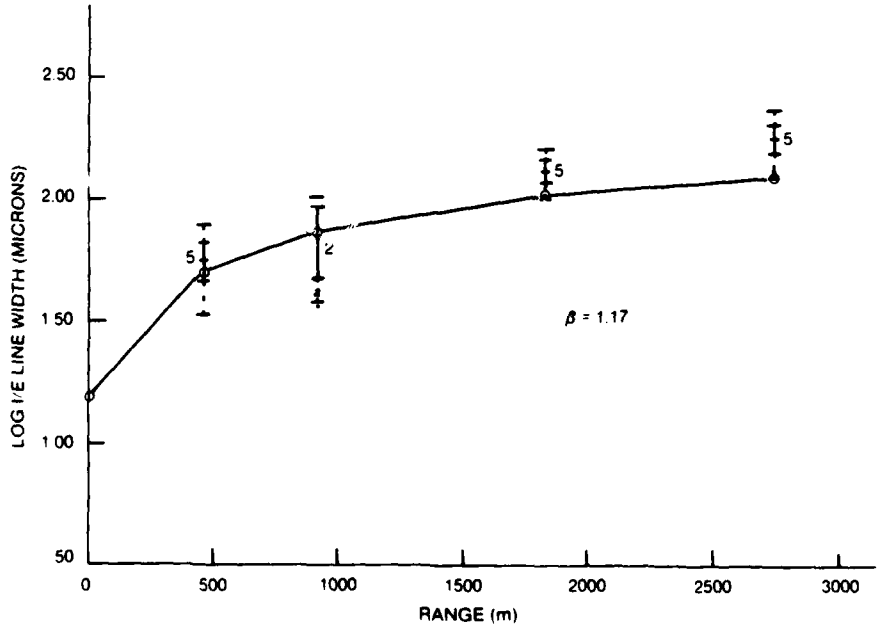

Figure 13b. Log Line Width (Microns)

Figure 13. Theoretical and Measured Line Widths for Series A

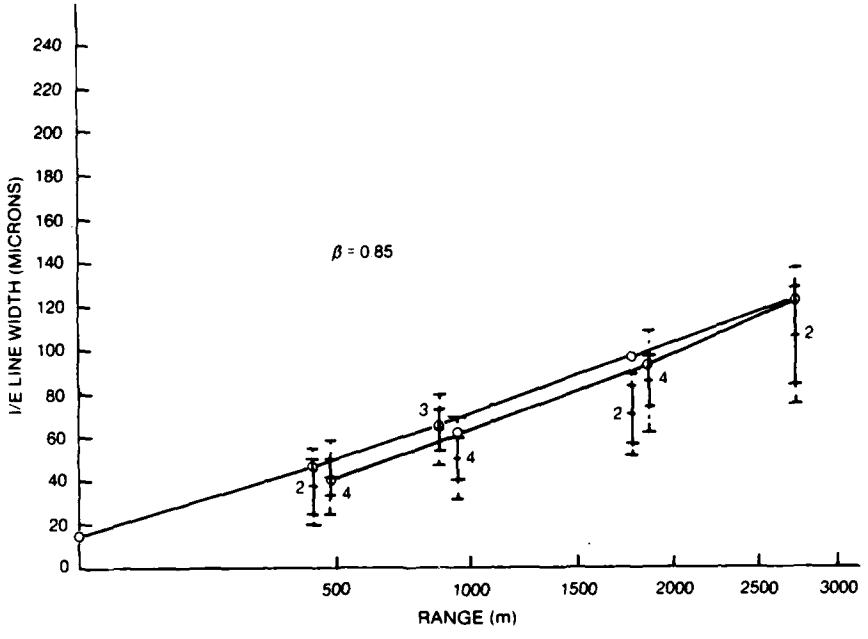

Figure 14a. Line Width (Microns)

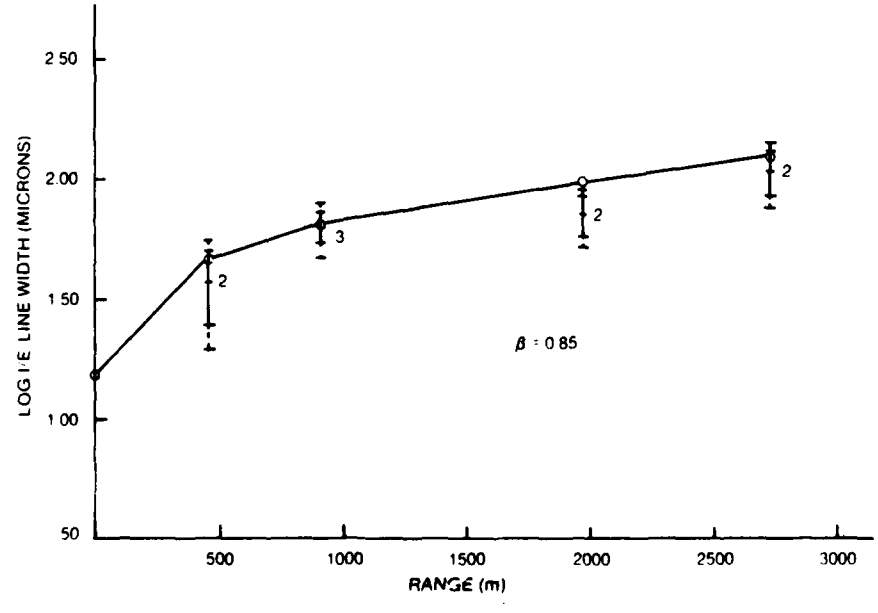

Figure 14b. Log Line Width (Microns) (Going)

Figure 14. Theoretical and Measured Line Widths for Series B

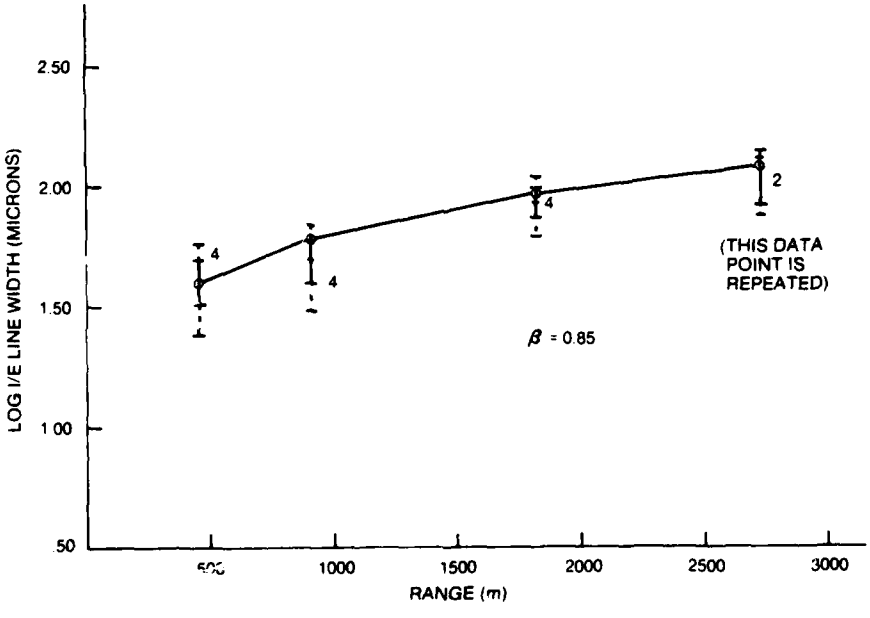

Figure 14c. Log Line Width (Microns) (Returning)

Figure 14. (Cont'd) Theoretical and Measured Line Widths for Series B

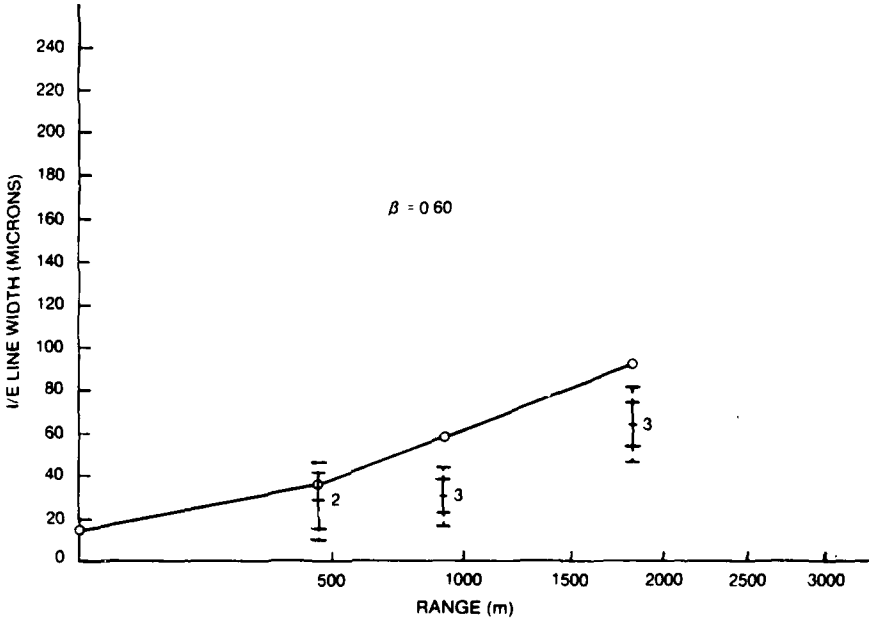

Figure 15a. Line Width (Microns)

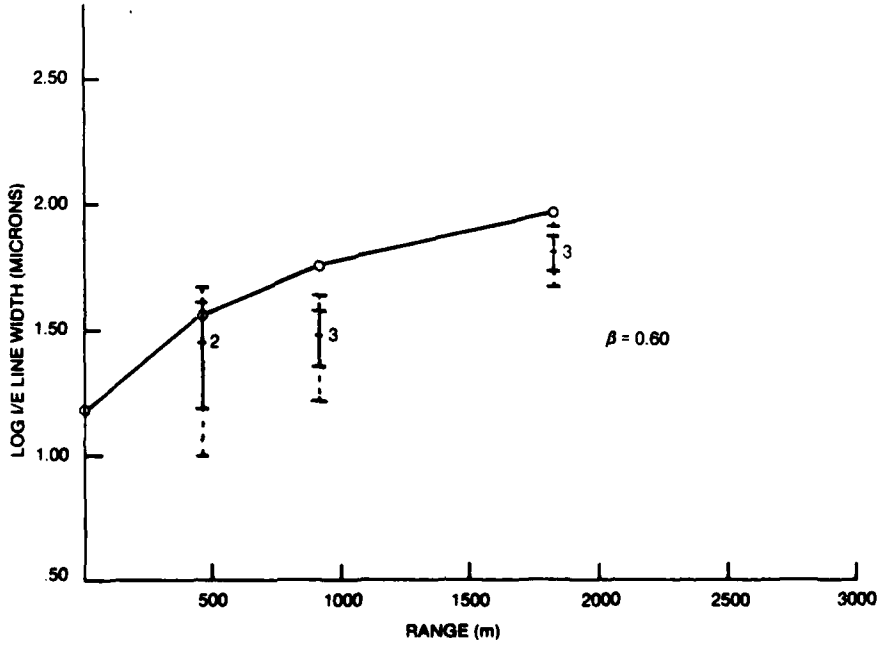

Figure 15b. Log Line Width (Microns)

Figure 15. Theoretical and Measured Line Widths for Series C

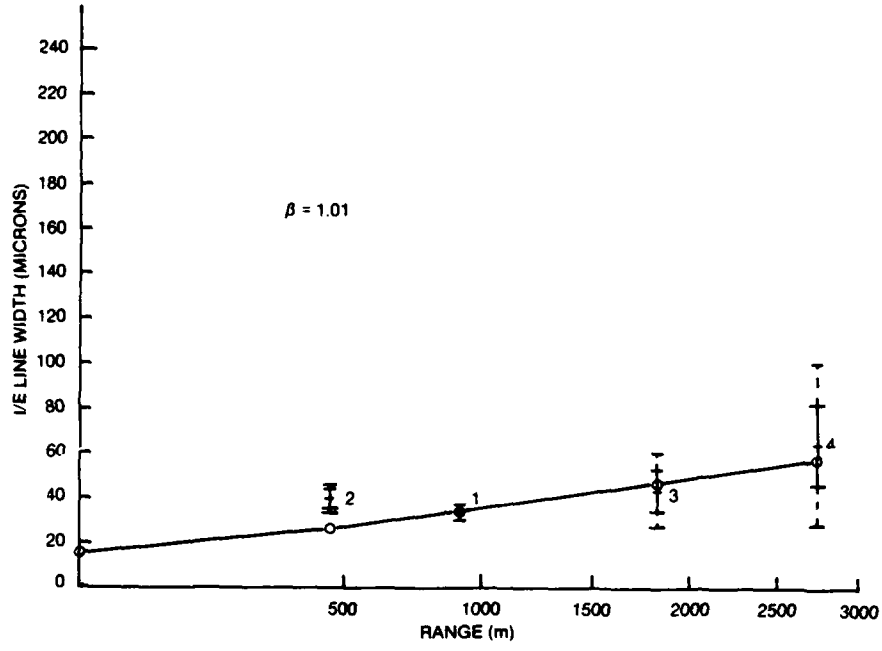

Figure 16a. Line Width (Microns)

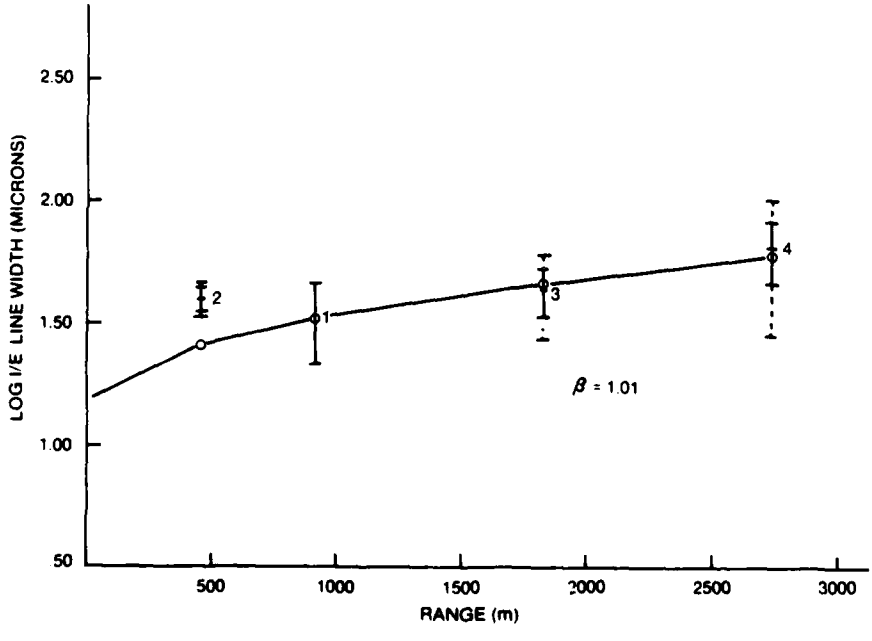

Figure 16b. Log Line Width (Microns)

Figure 16. Theoretical and Measured Line Widths for Series F

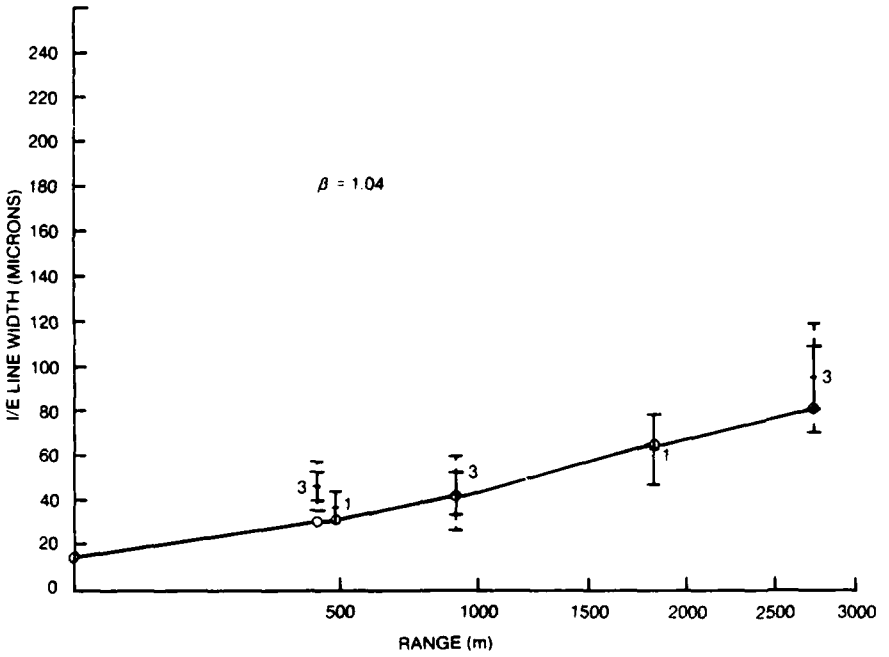

Figure 17a. Line Width (Microns)

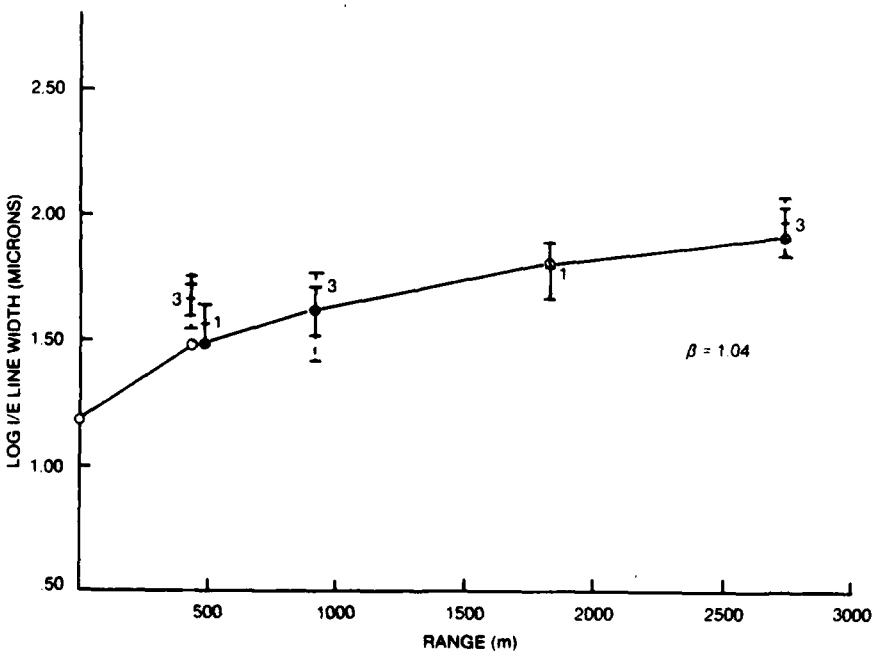

Figure 17b. Log Line Width (Microns)

Figure 17. Theoretical and Measured Line Widths for Series G

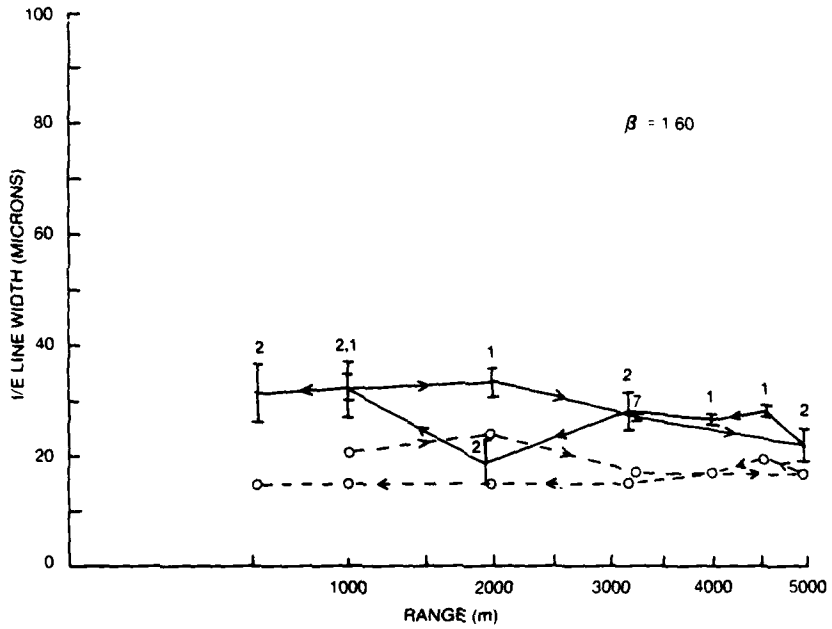

Figure 18. Theoretical and Measured Line Widths for Series H

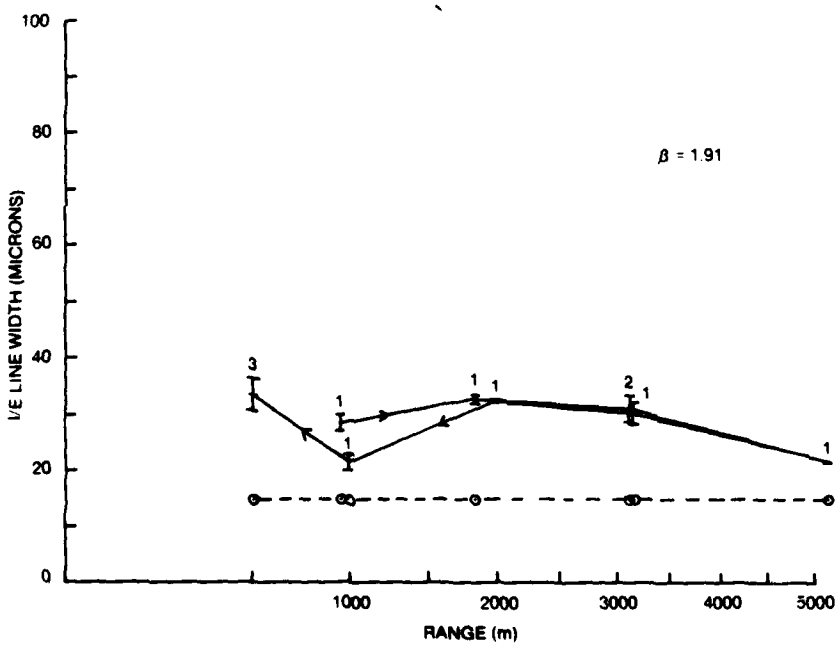

Figure 19. Theoretical and Measured Line Widths for Series I

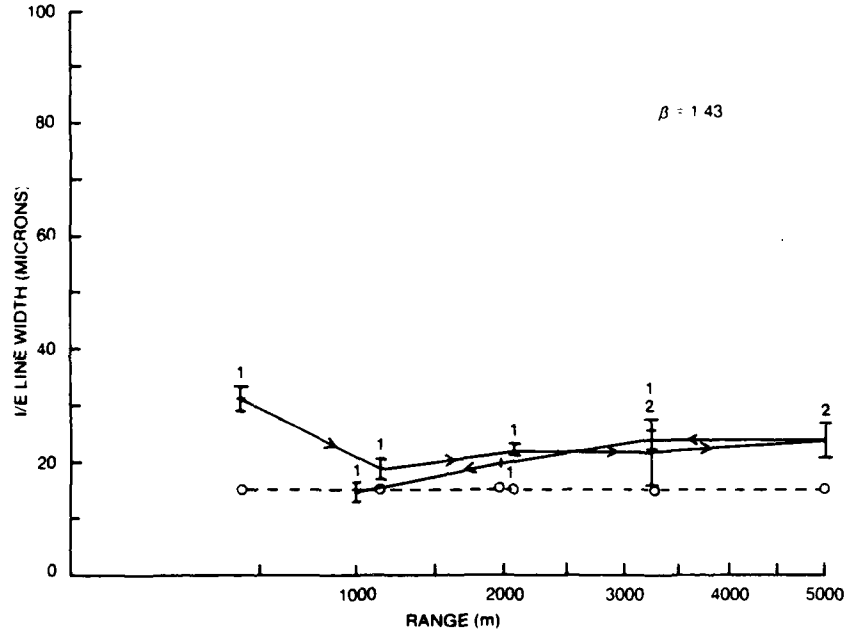

Figure 20. Theoretical and Measured Line Widths for Series J

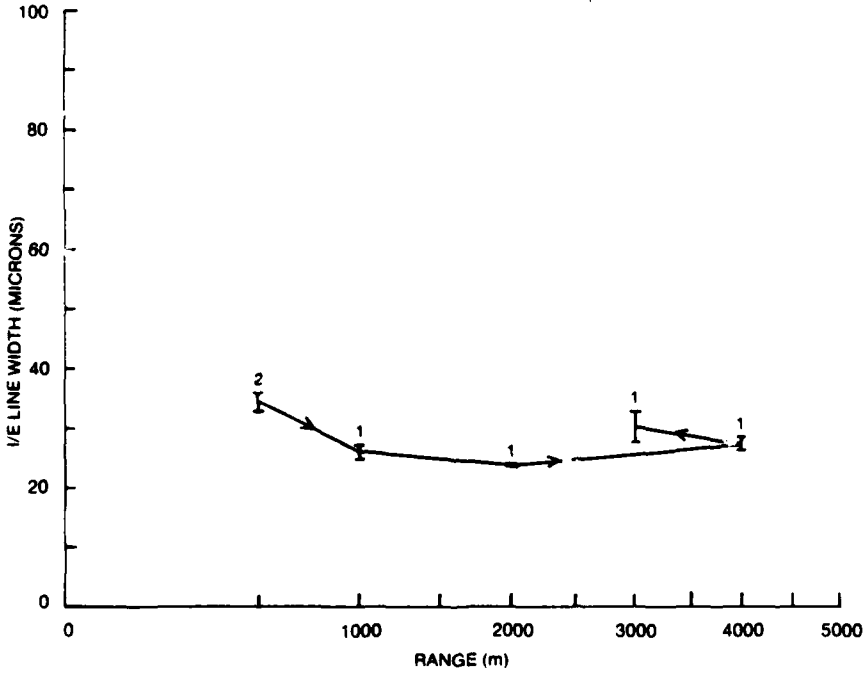

Figure 21. Measured Line Widths for Series K

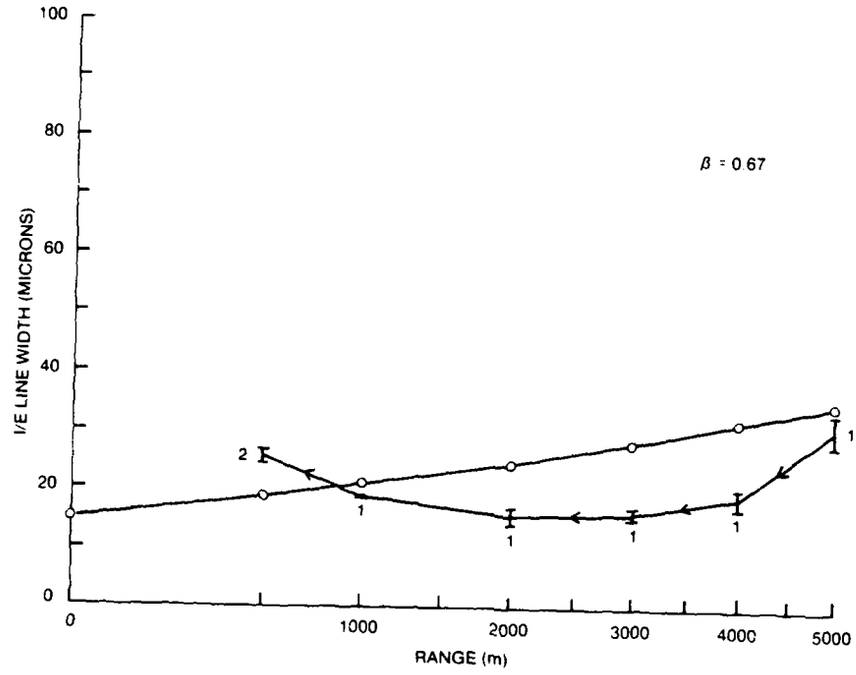

Figure 22. Theoretical and Measured Line Widths for Series L

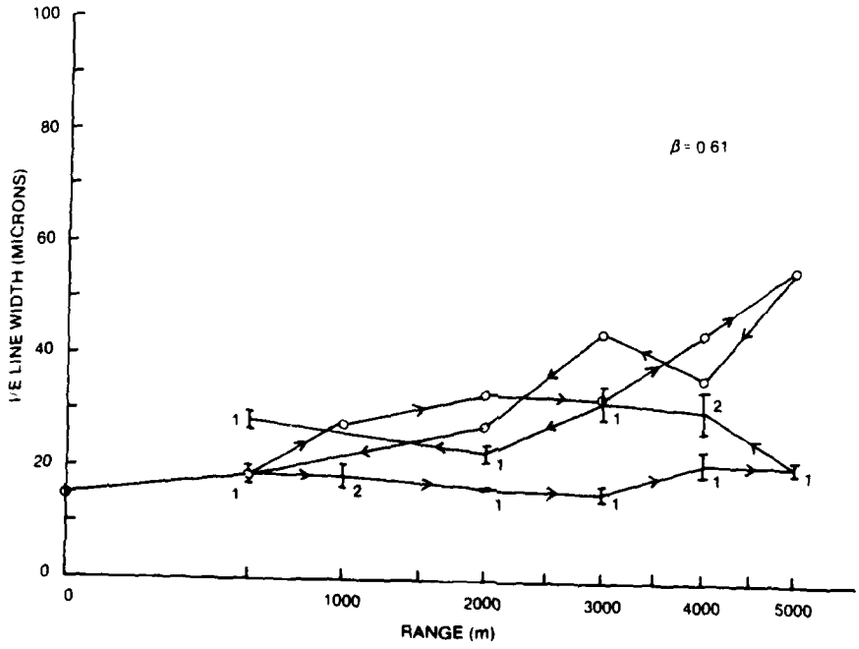

Figure 23. Theoretical and Measured Line Widths for Series M

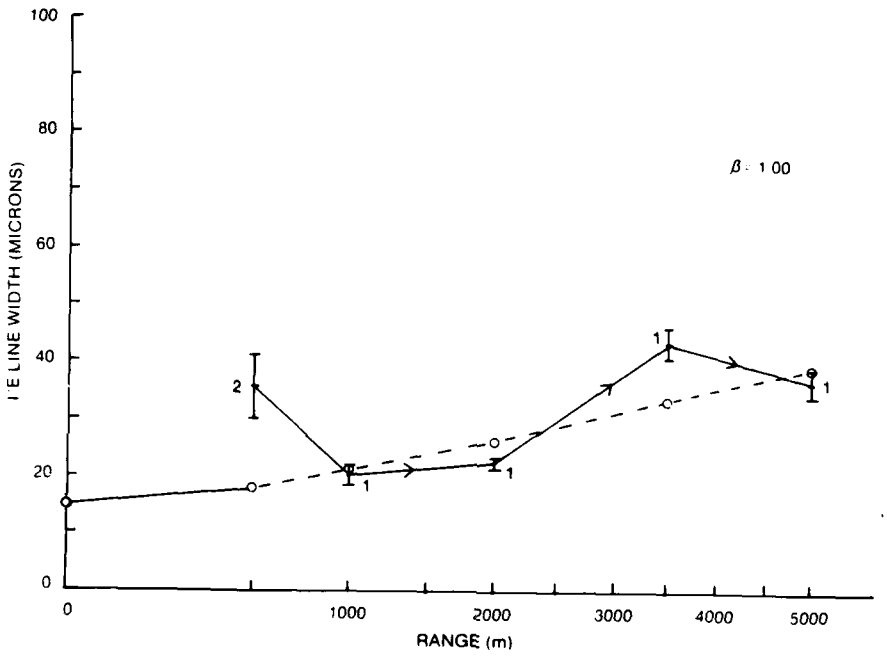

Figure 24. Theoretical and Measured Line Widths for Series N

REFERENCES

1. W. E. K. Middleton, *Vision Through the Atmosphere*, University of Toronto Press, Sections 4.1 to 4.4, 1952.

2. K. Davidson, T. Houlihan, C. Fairall, and G. Schacher, *Observations of the Temperature Structure Function Parameter, C_T^2, Over the Ocean*, Report No. NPS63-78-005, Naval Postgraduate School, Monterey, CA 93940, September 1978.

3. F. Replogle, Jr., "Measurements of the Effect of Refractive Irregularities in the Atmosphere on Imaging," NUSC Tech Memo No. 771196, Naval Underwater Systems Center, New London, CT 06320, 3 October 1977.

4. K. Davidson, et al., "Verification of the Bulk Method for Calculating Overwater Optical Turbulence," *Applied Optics* 20, No. 17, pp. 2919-2924, 1 September 1981.

5. R. Lutomirski and H. Yura, "Wave Structure Function and Mutual Coherence Function of an Optical Wave in a Turbulent Atmosphere," *Journal of the Optical Society of America*, 61, No. 4, p. 482, Equation (9b), April 1971.

6 .R. Lutomirski, et al., *Degradation of Laser Systems by Atmospheric Turbulence*, Equation (7.20), Report No. R-1171-ARPA/RC, June 1973.

7. H. Yura, "Short-term Average Optical-beam Spread in a Turbulent Medium," Journal of the Optical Society of America, 63, No. 5, p. 567, Equations (9) to (14), May 1973.

APPENDIX

COMPUTATION OF $C_n^2(z)$ FROM BULK METEOROLOGICAL MEASUREMENTS

From initial bulk meteorological measurements made at a height z′ we proceed to derive $C_n^2(z)$, where z is any height above the surface. This will be done for both stable and unstable atmospheres.

The first variable to be obtained is the surface roughness distance z_0 given by

$$z_0 = 10 \exp(-0.35/\sqrt{C_{DN}}),$$

where C_{DN} is obtained from the wind speed, U, at z′ from the tabulation

$C_{DN} \times 1000$	U(m/s)
$1.080\ U^{-0.15}$	0.3 to 2.2
0.770 + .086U	2.2 to 5.0
0.870 + .067U	5.0 to 8.0
1.200 + 0.25U	8.0 to 25.0

This leads to values of the drag coefficient C_{DN},

$$C_{DN}(U) = [0.35/\ell n(z'/z_0)]^2. \tag{A-1}$$

We then calculate a stability correction factor ξ_0', which is used in setting up scalar profiles of wind speed, temperature, and humidity. This is given by

$$\xi_0' = \frac{1.62z' \cdot (\Delta\theta + 6.2 \times 10^{-4} T \Delta_q)}{T \cdot \ell n(5 \times 10^{-4} z') \cdot C_{DN}(U) \cdot U^2}, \tag{A-2}$$

where the variables are measured at height z′.

From the stability correction factor the true atmospheric stability at height z′ is given implicitly by

$$\xi' = z'/L = \xi_0' \cdot \frac{[1 - \psi_1(\xi')/\ell n(z'/z_0)]^2}{1 - \psi_2(\xi')/\ell n(5 \times 10^4 z')}. \tag{A-3a}$$

For *stable* atmospheric conditions ($\xi_0' > 0$),

$$\psi_1(\xi') = -4.7\xi', \tag{A-3b}$$

and

$$\psi_2(\xi') = -6.5\xi',$$

and for *unstable* atmospheric conditions ($\xi_0' < 0$),

$$\psi_1(\xi') = 2\,\ell n[(1 + x)/2] + \ell n[(1 + x^2)/2] - 2\tan^{-1}(x) + \pi/2,$$

with

$$x = (1 - 15\xi')^{1/4},$$

and

$$\psi_2(\xi') = 2\,\ell n[(1 + \sqrt{1-9\xi'})/2].$$

For a stable atmosphere, (A-3a) and (A-3b) may be formulated as a quadratic function of $\xi'(z')$ and solved for ξ'. For an unstable atmosphere, (A-3a) and (A-3c) may be solved iteratively for ξ' by substituting first ξ_0' and then successively more accurate values of ξ' in the right-hand side of (A-3a). The resulting improved value of ξ' is calculated after each substitution.

We now require values for the temperature and humidity scaling parameters, T_* and Q_* (gm/m^3), respectively. They are given by

$$T_* = 0.47\Delta\theta/[\ell n(5 \times 10^4 z') - \psi_2(\xi')] \tag{A-4}$$

and

$$Q_* = 1.3\,q_* = 0.61\,\Delta q/[\ell n(5 \times 10^4 z') - \psi_2(\xi')]. \tag{A-5}$$

From this point we refer to the height z at which the turbulence will be observed and to the stability parameter

$$\xi(z) = z/L = z/z' \cdot \xi'(z).$$

From initial temperature and humidity difference data and the derived value of ξ we may now calculate structure functions for temperature and humidity, as well as the temperature-humidity covariance function. These are given by

$$C_T^2 = T_*^2 \cdot z^{-2/3} \cdot f(\xi), \tag{A-7a}$$

$$C_Q^2 = 0.6\,Q_*^2 \cdot z^{-2/3} \cdot f(\xi), \tag{A-7b}$$

$$C_{TQ} = 0.62\,T_*Q_* \cdot z^{-2/3} \cdot f(\xi), \tag{A-7c}$$

where the height dependence function f is given for a *stable* atmosphere by

$$f(\xi)_s = 4.9\,(1 + 2.4\xi^{2/3}),$$

and for an *unstable* atmosphere by

$$f(\xi)_u = 4.9\,(1 - 7\xi)^{-2/3}.$$

Finally, by combining the effects of temperature and humidity and relating them to variations in optical index, we obtain for the index structure function

$$C_n^2 = (79 \times 10^{-6} P/T^2)^2 \cdot (C_T^2 + 0.113\, C_{TQ} + 0.0031\, C_Q^2), \qquad \text{(A-8)}$$

where P is the air pressure in millibars and T is the absolute air temperature.

For an optical path having a varying height above the sea surface, it is useful to have an expression for C_n^2 giving an explicit height dependence. Combining (A-6), (A-7), and (A-8) yields

$$C_n^2 = (79 \times 10^{-6} P/T^2)^2 \cdot [T_*^2 + 0.070\, T_* Q_* + 0.0019\, Q_*^2]\, z^{-2/3} \cdot f(z/L). \qquad \text{(A-9)}$$

Initial Distribution List

Addressee	No. of Copies
CNO OP 009E (C. L. Heidler), OP 224C (CDR K. Stein)	2
NAVSEA 61Z51 (Carl Campbell)	1
NAVPGSCOL (Dr. E. Crittenden, Dr. K. L. Davidson, Dr. C. W. Fairall)	3
ONR (Dr. David Lewis, Dr. Paul Twitchell)	2
NASC Code 370C (Murray Schefer)	1
NAVELEX PME107-14 (E. Walsh)	1
NAVAVIONICFAC (James Russell)	1
NAVAIR 5473B (V. A. Seifert)	1
DTIC	12
DNL (R. Hillyer)	1

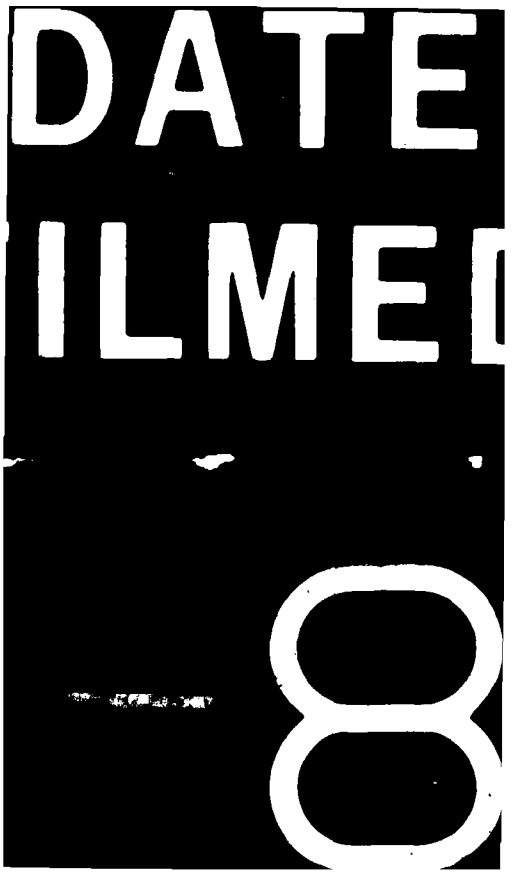
DATE
ILME
8